

CERTIFICATION OF APPROVAL

Analysis of Gas Turbine Blade Cooling System

by

Amir Hossein Ghanizadeh

A project dissertation submitted to the
Mechanical Engineering Programme
Universiti Teknologi PETRONAS
in partial fulfilment of the requirement for the
BACHELOR OF ENGINEERING (Hons)
(MECHANICAL ENGINEERING)

Approved by,

AP. Dr. Hussain H. AL-Kayiem

UNIVERSITI TEKNOLOGI PETRONAS

TRONOH, PERAK

November 2009

CERTIFICATION OF ORIGINALITY

This is to certify that I am responsible for the work submitted in this project, that the original work is my own except as specified in the references and acknowledgements, and that the original work contained herein have not been undertaken or done by unspecified sources or persons.

Amir Hossein Ghanizadeh

ABSTRACT

Gas turbine engines are designed to continuously and efficiently convert the energy of fuel into useful power. Gas turbines have been developed into very reliable, high performance engines (high ratio of power output to weight, high efficiency and low maintenance costs).

As the turbine inlet temperature increases, the heat transferred to the turbine blade also increases. The operating temperatures are far above the permissible metal temperatures. Therefore, there is a critical need to cool the blades for safe operation. The cooling methods currently implemented in the turbine industry can be classified into two types: internal cooling and external cooling.

In the present work the internal cooling of a gas turbine blade is analyzed. The blade has a rectangular $9\text{mm} \times 18\text{mm}$ compressed air channel along the blade span. Finite-Difference method is used to predict temperature distribution for blade cross section at different heights from the root. Effect of compressed air mass flow rate, inlet temperature and the temperature of combustion gasses have been considered. The investigations are carried out for both smooth and two opposite ribbed-walls channels. The results are presented and discussed as temperature distribution in various sections of the blade and the comparison between ribbed and smooth channel based on Nu values. Also, various ribs configurations have been considered in the analysis. Results at rib angles, α of 90° , 60° , 45° and 30° and ribs blockage ratios, e/D_h ranging from 0.042 to 0.078 are compared in terms of Nu and friction factor, f . It is found that maximum Nu number occurs when 60° ribs are introduced in the channel. An enhancement of 149.45% is achieved with penalty of increase in the friction factor by 114.5%.

ACKNOWLEDGMENTS

I would like to take this opportunity to thank all the people who have given help, support and encouragement to me during my Final Year Project.

My supervisor Dr. Hussain H. AL-Kayiem deserves special thanks. Dr. Hussain provided many hours of guidance and support and was always willing to discuss my project. I am very grateful for all his help. I could not have asked for a better supervisor than Dr. Hussain. His attentions to details of my research, and his advice and friendship have made my FYP an extremely rewarding experience. His passion for mechanical engineering has really inspired me.

I owe special thanks to the other lecturers of Mechanical Engineering Department for all their suggestions, comments and discussions for improvement of this work during seminars and presentations, specifically to Dr. Zainal Ambri Bin Abdul Karim for his comments on dissertation first draft.

Last but not the least; I would like to thank my parents who provided support for me even though I was half a world away. Without my family's support, I would have not been able to achieve my goals.

TABLE OF CONTENTS

CERTIFICATION	i
ABSTRACT	ii
ACKNOWLEDGMENTS	iii
CHAPTER 1 INTRODUCTION	1
1.1 GAS TURBINE BACKGROUND.....	1
1.2 COOLING TECHNIQUES.....	2
1.3 PROBLEM STATEMENT.....	4
1.4 OBJECTIVES.....	4
1.5 SCOPE OF STUDY.....	4
CHAPTER 2 LITERATURE RIVIEW AND THEORY	5
2.1. THEORY.....	5
2.2. REVIEW ON FILM COOLING FLOW STRUCTURE.....	6
2.3 FACTORS AFFECTING FILM COOLING.....	7
2.3.1 Blowing ratio.....	8
2.3.2 Mainstream Acceleration.....	9
2.3.3 Injection Hole Geometry.....	9
2.3.4 Coolant-to-Mainstream Density Ratio.....	10
2.3.5 Coolant Supply Geometry.....	11
2.3.6 Mainstream Turbulence.....	12
2.3.7 Partial Hole Blockage.....	12
2.4 REVIEW ON EFFECT OF RIBS IN INTERNAL COOLING....	14
2.5 EFFECTS OF ROTATION ON COOLANT PASSAGE.....	16
CHAPTER 3 METHODOLOGY	24
3.1 ANALYSIS TECHNIQUES.....	24
3.2 WORK FLOW CHART.....	26
3.3 GANTT CHART.....	26
CHAPTER 4 PREPARATIONS AND DISCUSSION OF RESULTS	27
4.1 NODAL EQUATIONS.....	28
4.2 RESULTS FOR SMOOTH CHANNEL.....	31
4.3 RESULTS FOR RIBBED CHANNEL.....	40
4.3.1 Introducing Orthogonal Ribs ($\alpha = 90^\circ$).....	42
4.3.2 Introducing 60° Ribs.....	44
4.3.3 Introducing 45° Ribs.....	46
4.3.4 Introducing 30° Ribs.....	48
4.3.4 Comparison between Different Rib Angles.....	50
4.4 DISCUSSION ON THE RESULTS.....	51
CHAPTER 5 CONCLUSION AND RECOMMENDATION	55
REFERENCES	57

LIST OF FIGURES

Figure 1.1: Schematics of a turbojet engine (Rolls Royce, 1973)	1
Figure 1.2: A nozzle guide vane with internal cooling (Rolls Royce, 1973).....	2
Figure 1.3: protective film layer made by coolant injection (adopted from Mohammed S. Altorairi, 2003)	3
Figure 1.4: A typical film cooled turbine blade (Metherwan P.Boyce, 2002).....	3
Figure 2.1: Sketch of jet structure based on experimental observations at high ($M = 2.0$) blowing ratios, [Andreopoulos and Rodi (1983)].	6
Figure 2.2: Sketch of jet structure based on experimental observations at low ($M = 0.5$) blowing ratios, [Andreopoulos and Rodi (1983)]	7
Figure 2.3: Effect of blowing ratio on centerline adiabatic effectiveness for simple angle injection holes inclined at 35 degrees, [Goldstein (1974)]	8
Figure 2.4: Effect of blowing ratio on the heat transfer coefficient ratio for simple angle injection holes inclined at 35 degrees, [Hey et al (1985)]	9
Figure 2.5: Effect of blowing ratio on the laterally average adiabatic effectiveness for different density ratios, [Pedersen et al (1977)].....	11
Figure 2.6: Effect of freestream turbulence on the centreline adiabatic effectiveness,	12
Figure 2.7: Micrograph showing deposits of foreign material in a film cooling hole, [Bogard et al (1998)].....	12
Figure 2.8: Flow patterns as a function of P/e , from [Webb et al. (1971)].....	15
Figure 2.9: Conceptual view of a two-pass rotating coolant flow distribution by [Han et al. (1993)].....	17
Figure 2.10: Predicted secondary flow, axial flow, and temperature distribution in a rotating square channel with radial outward flow, collected in [Han et al. (2000)]	18
Figure 2.11: Multipass rotating channel with 45° ribs used by [Johnson et al. (1994)] to simulate a turbine rotor blade coolant passage.	19
Figure 2.12: Conceptual view of the secondary flow vortices induced by rotation and channel orientation in a two-pass rectangular channel (dash lines: rotation-induced vortices; solid lines: rib-induced vortices) from [Azad et al. (2001)].....	22

Figure 2.13: Conceptual view of the secondary flow vortices induced by rotation and channel orientation in a two-pass rectangular channel (dash lines: rotation-induced vortices; solid lines: rib-induced vortices) from [Al-Hadhrami et al. (2002)].	23
Figure 2.14: Outward flow rectangular test section with smooth walls and 45° parallel angled ribs on leading and trailing surfaces by [Griffith et al. (2001)].	23
Figure 4.1: GT blade in building 18.	27
Figure 4.2: Cross-section of the modeled GT blade and correspondence meshing around the internal air channel.	27
Figure 4.3: 3-D model of the blade	28
Figure 4.4: Heat transfer in an infinitesimal small control volume	28
Figure 4.5: Conduction to an interior node from its adjoining nodes (Dewill et al., 2007)	29
Figure 4.6: Temperature (K) distribution in the cross section of GT blade surrounding the cooling passage at root of the blade.	32
Figure 4.7: Temperature (K) distribution in the cross section of the second segment (H=5.25 to H=10.5 cm) of GT blade surrounding the cooling passage.	34
Figure 4.8 : Temperature (K) distribution in the cross section of the third segment (H=10.5 to H=15.75 cm) of GT blade surrounding the cooling passage.	35
Figure 4.9 : Temperature (K) distribution in the cross section of the fourth segment (H=15.75 to H=21 cm) of GT blade surrounding the cooling passage.	35
Figure 4.10 : Air outlet temperature (K) for different mass flow rates (kg/s) for smooth channel	36
Figure 4.11 : Convection coefficient ($W/m^2 \cdot K$) for different air mass flow rates (kg/s) in smooth channel	37
Figure 4.12 : Local convection coefficient in the smooth channel	37
Figure 4.13 : Temperature (K) distribution along top blade surface (H=15.75 to H=21 cm).	38
Figure 4.14: Temperature (K) distribution along bottom blade surface (H=15.75 to H=21 cm).	38
Figure 4.15 : Temperature distribution along the adiabat line.	39
Figure 4.16 : Temperature distribution along the chamber of blade.	39

Figure 4.17: Friction factor and heat transfer correlation in narrow-aspect ratio rectangular ribbed channels (Han et al., 1989)	42
Figure 4.18: Temperature (K) distribution in the cross section of GT blade surrounding the 90° ribbed cooling channel at root of the blade.	44
Figure 4.19: Temperature (K) distribution in the cross section of GT blade surrounding the 60° ribbed cooling channel at root of the blade.	46
Figure 4.20: Temperature (K) distribution in the cross section of GT blade surrounding the 45° ribbed cooling channel at root of the blade.	48
Figure 4.21: Temperature (K) distribution in the cross section of GT blade surrounding the 30° ribbed cooling channel at root of the blade.	49

LIST OF TABLES

Table 3-1: FYPII Gantt chart	26
Table 4-1: Summary of nodal finite-difference equations (Dewill et al., 2007).....	30
Table 4-2: Friction factor, Nu number and h value for different rib blockage ratios, e/D_h when $\alpha=90^\circ$	44
Table 4-3: Friction factor, Nu number and h value for different rib blockage ratios, e/D_h when $\alpha=60^\circ$	45
Table 4-4: Friction factor, Nu number and h value for different rib blockage ratios, e/D_h when $\alpha=45^\circ$	47
Table 4-5: Friction factor, Nu number and h value for different rib blockage ratios, e/D_h when $\alpha=30^\circ$	49
Table 4-6: Comparison between different rib angles for maximum and minimum temperature, heat transfer per length and increment in air temperature when leaving the channel.	50
Table 4-7: Comparison between effect of <i>thermal conductivity</i> and <i>conduction coefficient</i> on the blade cooling in smooth channel.	51
Table 4-8: Variations of max & min temperature along the height of the blade.	52

CHAPTER 1

INTRODUCTION

In this Chapter, an overview of gas turbine engines is given. The significance of turbine entry temperature, the necessity of cooling the turbine blades and different types of cooling techniques are also discussed. This introduction then concludes with the objectives and scope of study of this work.

1.1 GAS TURBINE BACKGROUND

Gas turbine engines are designed to continuously and efficiently convert the energy of a fuel into useful power; either mechanical power or the high-speed thrust of a jet. In 1913, Lorin patented a jet propulsion engine; however, his engine was not manufactured (Rolls Royce, 1973). Before the Second World War, serious development of the shaft-power gas turbine began, but attention was soon focused on the turbojet engine (Cohen et al., 1996). In 1930, Boveri developed the first useful gas turbine (Bathie, 1995) and Whittle was granted a patent for using a gas turbine to produce a propulsive jet (Rolls Royce, 1973). Since then, gas turbines have been developed into very reliable, high performance engines (high ratio of power output to weight, high efficiency and low maintenance costs). Gas turbines are now widely used in power plants, marine industries and aircraft propulsion. They are used in powering boats and trains and are also being tested for use in buses and trucks and even as a power plant for an automobile.

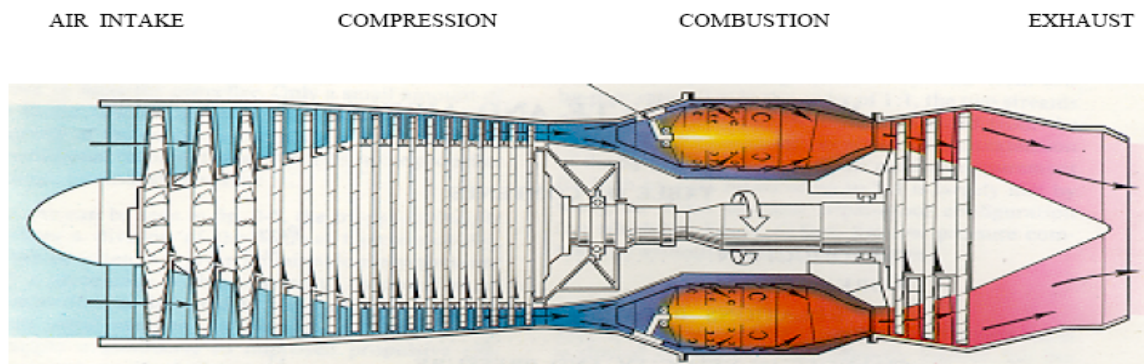


Figure 1.1: Schematics of a turbojet engine (Rolls Royce, 1973)

Developments in turbine cooling technology play a critical role in increasing the thermal efficiency and power output of advanced gas turbines [Aminossadati S.M. and Mee D.J., 1995].

1.2. COOLING TECHNIQUES

To achieve an optimum cooling system, researchers focus on various innovative cooling techniques. Depending on the nature of the coolant flow, the cooling methods currently implemented in the turbine industry can be classified into two types: internal cooling and external cooling.

In the first type cooler, air is bled from the compressor stage and then passed through internal passages incorporated into blade designs for this purpose (Fig.1.2). This is the most common technique and is called enhanced passage cooling. For maximum heat absorption, the air is also allowed to impinge on the internal wall of the blade. This technique is called impingement cooling [Aminossadati S.M. and Mee D.J., 1995].

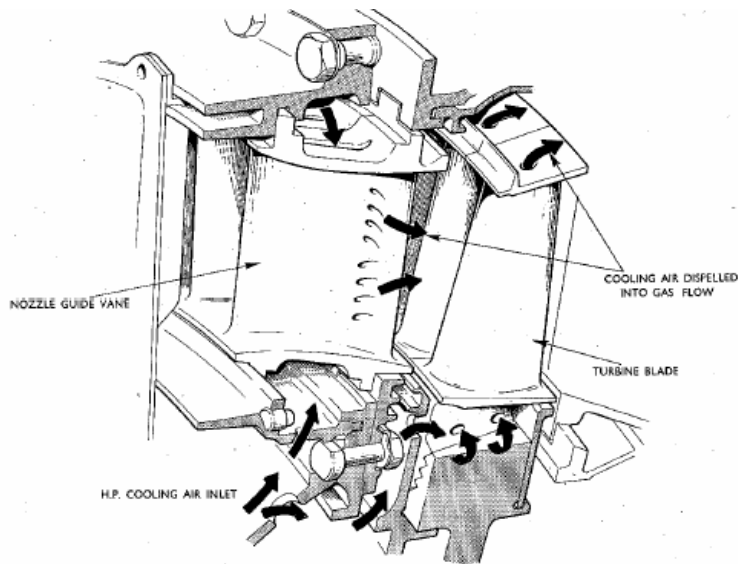


Figure 1.2: A nozzle guide vane with internal cooling (Rolls Royce, 1973)
(Coolant ejection through a row of holes on the pressure side near the trailing edge)

In external cooling, air is bled from the compressor stage, ducted through the internal chambers of the turbine blades, and then discharged through small holes/ slots on the

blade outer walls. This air provides a thin, cooler, insulating film along the external surface of the turbine blade, due to which the method is called “film cooling” (Fig 1.3 & 1.4). That film provides protection and thus increases the life of the blade. This life may be reduced by 50% if the blade’s operating temperature was off the maximum design temperature by 10 °C [Mohammed S. Altorairi, 2003].

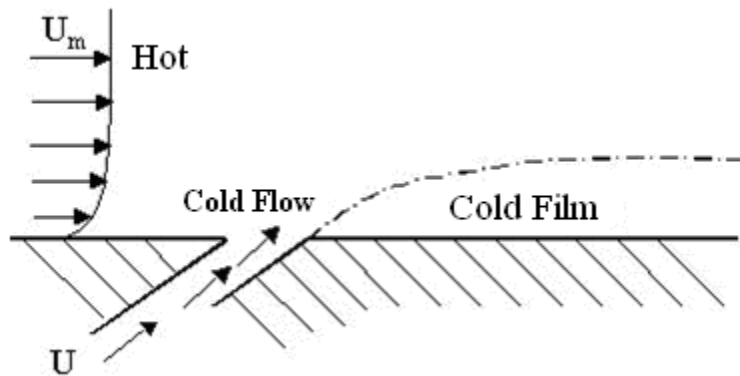


Figure 1.3: protective film layer made by coolant injection (adopted from Mohammed S. Altorairi, 2003)

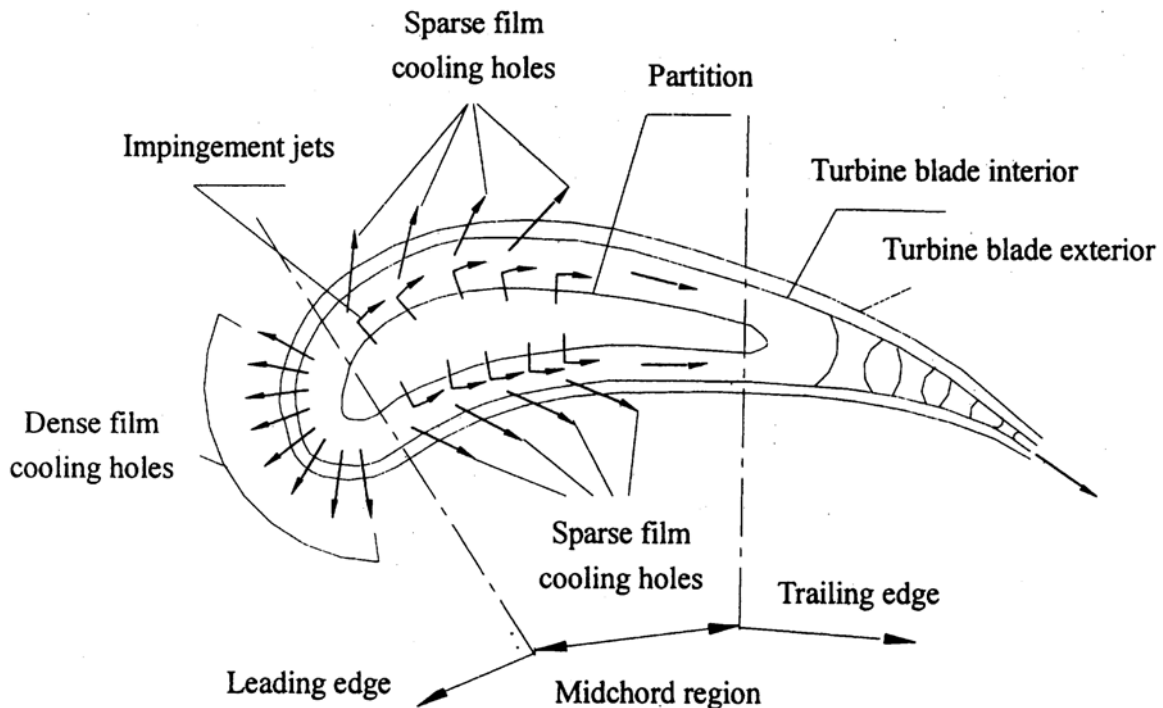


Figure 1.4: A typical film cooled turbine blade (Metherwan P.Boyce, 2002).

1.3. PROBLEM STATEMENT

As the turbine inlet temperature increases, the heat transferred to the turbine blade also increases. The level and variation in the temperature within the blade material, which cause thermal stresses, must be limited to achieve reasonable durability goals. The operating temperatures are far above the permissible metal temperatures. Therefore, there is a critical need to cool the blades for safe operation. The blades are cooled with extracted air from the compressor of the engine. Since this extraction incurs a penalty on the thermal efficiency and power output of the engine, it is important to understand and optimize the cooling technology for a given turbine blade geometry under engine operating conditions. Gas turbine cooling technology is complex and varies between engine manufacturers.

1.4. OBJECTIVES

Objectives of this project are as follows:

- To establish mathematical model for air flow through the gas turbine blades representing flow dynamics and heat transfer process.
- To convert the mathematical model to computer program and investigate the blade cooling performance at various operational conditions and configuration in order to optimize it.
- To recommend the best configuration according to the results.

1.5 SCOPE OF STUDY

A review of the available material on cooling techniques for gas turbine applications will be presented. Some works are available in this area with studies having been carried out, particularly in the past fifteen to twenty years. Heat transfer and fluid dynamics relations and equations will be chosen to build a mathematical model of air flow through turbine blades. The mathematical model will be converted to a computer program to obtain compare and interpret the results and findings.

CHAPTER 2

LITERATURE RIVIEW AND THEORY

In this chapter a review of the available material on film cooling and internal cooling for gas turbine applications is presented. Some works are available on this area with studies having been carried out, particularly in the past fifteen to twenty years.

2.1. THEORY

Going through the literature, there are a series of definitions that have been developed and used extensively in this particular area. So, to use previous research works it is important to understand them.

The primary aim for the majority of these studies has been to maximize the adiabatic effectiveness (film effectiveness). This parameter is dependent upon three temperatures, that of the mainstream, coolant and of the surface being cooled, it is defined as:

$$\xi = \frac{T_{aw} - T_m}{T_c - T_m}$$

The adiabatic effectiveness measures the efficiency of a coolant film, where a value of unity indicates that the temperature of the surface being cooled is the same as the coolant temperature. Heat transfer coefficients are also an important parameter in determining the effectiveness of film cooling, the objective of film cooling being to achieve a low heat transfer coefficient from the surrounding hot mainstream to the surface, and a large effectiveness on the surface. Results are often expressed in terms of the heat transfer coefficient ratio, defined as:

$$\frac{h_1}{h_0} = \left(\frac{q_1}{q_0}\right) \left(\frac{T_m - T_w}{T_{aw} - T_w}\right)$$

Another important property is the blowing ratio, this relates the density and velocity of the mainstream and coolant flows, it is defined as:

$$M = \frac{\rho_c U_c}{\rho_m U_m}$$

The effect of this parameter on the adiabatic effectiveness is the primary interest for a number of studies due to its significant impact on the film cooling performance.

2.2. REVIEW ON FILM COOLING FLOW STRUCTURE

The behavior of jets injected into a cross flow has been the subject of numerous studies and is now well documented, Andreopoulos and Rodi (1983), Crabb et al (1981) and Moussa et al (1977). Immediately after penetration into the mainstream flow the jet behaves like a flexible body, the structure of which is strongly three dimensional. At some distance from the jet exit, two counter-rotating vortices are formed which produce the classic ‘kidney’ shape of the injection (Fig 2.1). The creation of these vortices is connected to viscous layers in the injection tube, their strength and impact on the flow depending heavily on the size of the boundary layer in the injection tube.

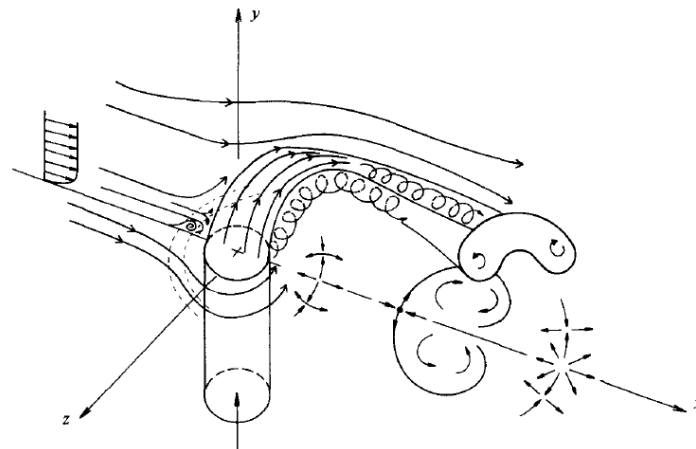


Figure 2.1: Sketch of jet structure based on experimental observations at high ($M = 2.0$) blowing ratios, [Andreopoulos and Rodi (1983).]

The deceleration of the external boundary layer as it interacts with the jet injection induces a horseshoe vortex which wraps around the jet; this flow is then entrained by the jet and begins to move upward from the wall (Fig 2.2). At smaller blowing ratios where

the penetration of the jet into the mainstream flow is low the jet bends over very quickly and attaches to the wall, this behavior is also observed when the injection angle relative to the mainstream flow direction is small.

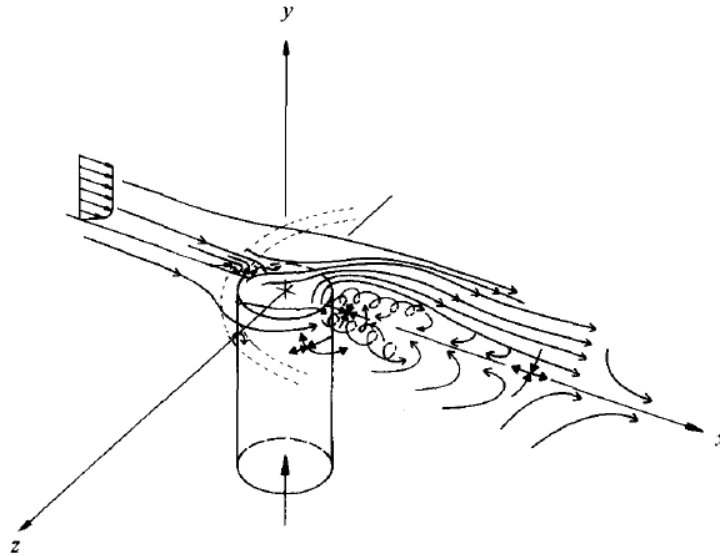


Figure 2.2: Sketch of jet structure based on experimental observations at low ($M = 0.5$) blowing ratios, [Andreopoulos and Rodi (1983)]

2.3 FACTORS AFFECTING FILM COOLING

A review of literature prior to 1971 on flat surface film cooling is presented in Goldstein (1971), the effects on film cooling performance of geometric and flow characteristics are described. The primary benefit of flat surface studies is the relative ease with which they can be carried out, slight corrections can then be made so the results can be applied to more complex geometries and ultimately actual engine design. Based on the literature following are parameters effecting film cooling as supported by Green (2007).

- Blowing ratio
- Injection hole geometry
- Mainstream acceleration
- Coolant to mainstream density ratio
- Coolant supply geometry
- Mainstream turbulence

- Partial hole blockage

2.3.1 Blowing ratio

Goldstein et al (1974) presented results detailing the effect of blowing ratio on the adiabatic effectiveness for a row of simple injection holes inclined at 35 degrees. At lower blowing ratios (e.g. $M < 0.5$) the adiabatic effectiveness displays a predictable pattern of simply increasing as the blowing ratio is increased. (Look at the figure below).

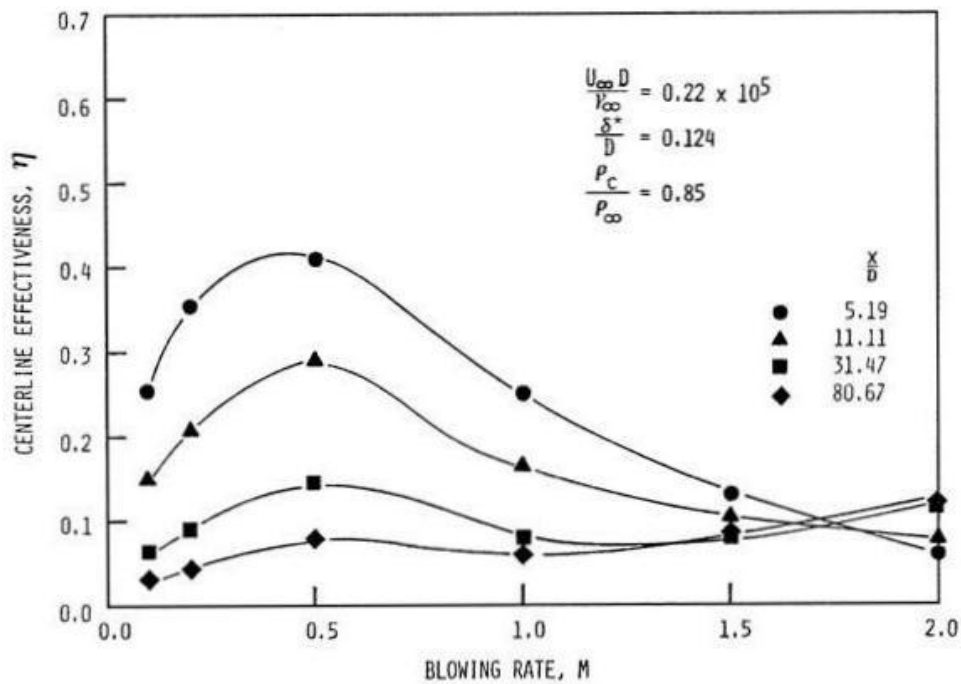


Figure 2.3: Effect of blowing ratio on centerline adiabatic effectiveness for simple angle injection holes inclined at 35 degrees, [Goldstein (1974)]

Hay et al (1985) carried out studies of injection holes inclined at 35 degrees (Fig 2.4). For all of the studies the heat transfer coefficient ratio was found to increase as the blowing ratio was increased. At lower blowing ratios the heat transfer coefficient was found to be approximately equal to unity regardless of the axial position from the point of injection, as the blowing ratio was increased the heat transfer coefficient also increased, particularly near the injection region (i.e. $x/D < 10$). This trend was also observed for a 90 degree injection angle (i.e. normal to the mainstream flow); however the effect of axial location was much stronger for the 90 degree injection compared to the 35 degree injection. In the case of a 35 degree angle of injection, because the jet penetrates into the mainstream flow at an angle

closer to the surface, the possibility of jet liftoff is greatly reduced resulting in the lower heat transfer coefficient ratios.

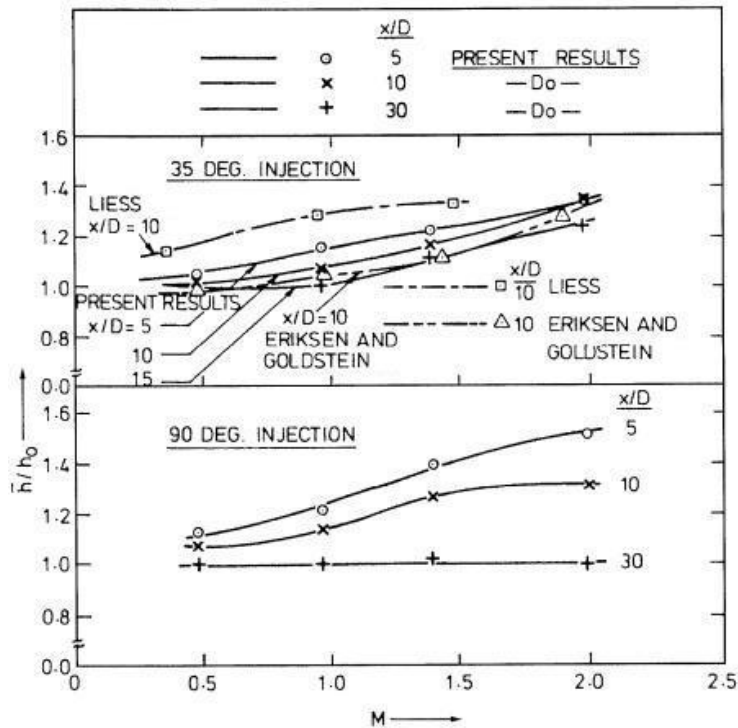


Figure 2.4: Effect of blowing ratio on the heat transfer coefficient ratio for simple angle injection holes inclined at 35 degrees, [Hey et al (1985)]

2.3.2 Mainstream Acceleration

Limited data is available in the open literature analyzing the effect of mainstream acceleration on film cooling performance. Ammari et al (1991) presented heat transfer coefficient ratios downstream of a row of film coolant holes analyzing the effect of mainstream acceleration; the heat transfer coefficient ratios were found to reduce by approximately 25% in the cases where mainstream acceleration was applied, obviously varying with different blowing ratios.

2.3.3 Injection Hole Geometry

Ligrani et al (1994a, b) presented results comparing single angle holes with compound angle holes. Results clearly show that the compound angle injection holes provide a

higher adiabatic effectiveness than the simple angle injection holes. The reason for this is an increase in the lateral momentum of the jet which results in a larger amount of lateral spreading when compared to the single angle injection. The injection holes in this case were aligned at 35 degrees in the Streamwise direction with the compound angle varied between 45 and 90 degrees in the spanwise direction. Increasing the spanwise angle to 90 degrees was found to increase the adiabatic effectiveness due to increased lateral spreading of the coolant jets.

Sen et al (1996) has also analyzed the effect of compound angle injection on the heat transfer coefficient ratio. The general trend in the results was for a higher heat transfer coefficient ratio when using compound angle injection holes over simple angle injection holes. The compound angle injection results in an increased reaction with the mainstream flow, this gives rise to an increase in the local turbulence and consequently leads to a higher heat transfer coefficient ratio; this effect is generally enhanced as the blowing ratio is increased (the maximum blowing ratio in the study was 3.0).

2.3.4 Coolant-to-Mainstream Density Ratio

The effect of the coolant-to-mainstream density ratio on the adiabatic effectiveness was documented by Pedersen et al (1977). Experiments were carried out on a single row of coolant holes inclined at 35 degrees in the mainstream flow direction; density ratios ranging from 0.75 to 4.17 were studied (Fig 2.5). It was found that density ratios less than unity gave a lower adiabatic effectiveness than those obtained using a high density ratio. Increasing the blowing ratio had a negative effect on the adiabatic effectiveness at the lower density ratios. This is due to the injection jet velocity being higher at lower density ratios, resulting in a greater penetration of the jet into the mainstream flow.

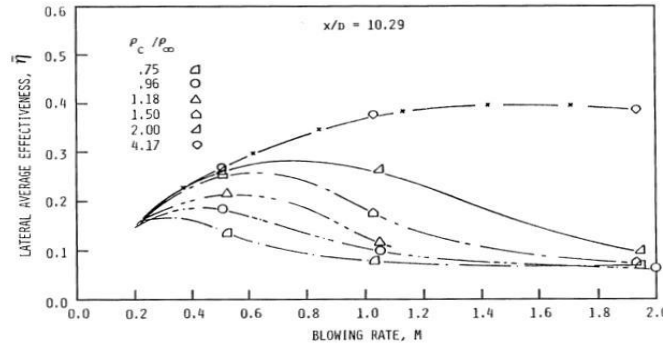


Figure 2.5: Effect of blowing ratio on the laterally average adiabatic effectiveness for different density ratios, [Pedersen et al (1977)]

Ammari et al (1990) also presented results showing the effect of cool-to-mainstream density ratio on the heat transfer coefficient ratio. It was observed that lower density ratios gave an increase in the heat transfer coefficient ratio; this is due to the increased momentum of the jet and its greater penetration into the mainstream flow. For lower blowing ratios (i.e. $M < 0.8$) the density ratio effect is confined to the stagnation region directly in lee of the jet, the effect becoming less pronounced as the distance from the point of injection is increased. For higher blowing ratios a change in the density ratio results in a significant impact on the results, producing a lower heat transfer coefficient ratio.

2.3.5 Coolant Supply Geometry

Hole supply geometry dictates how the coolant enters the film hole and the characteristics of the coolant within the supply hole. Leylek and Zerkle (1994) showed that short injection holes are subject to a ‘jetting’ effect. This occurs when the coolant jet velocity profile is not uniformly distributed across the exit plane, resulting in relatively high velocities for a substantial part of the coolant increasing its penetration into the mainstream flow. The effect of injection hole length on the film cooling performance for a row of five compound injection holes, orientated in the streamwise direction, was investigated by Seo et al (1998). Increasing the L/D ratio was found to result in an increase in the adiabatic effectiveness; this was attributed to a skewing of the velocity profile at low L/D ratios towards the upstream side of the injection hole.

2.3.6 Mainstream Turbulence

Film cooling flow characteristics can be severely affected by the level of turbulence in the mainstream. Bons et al (1996) documented the effect of mainstream turbulence on the adiabatic effectiveness (Fig 2.6). At relatively low blowing ratios (e.g. $M = 0.75$) and low mainstream turbulence (e.g. 0.9%) reasonably high values of adiabatic effectiveness are recorded in the vicinity of the coolant jets, decreasing steadily as the distance from the point of injection was increased.

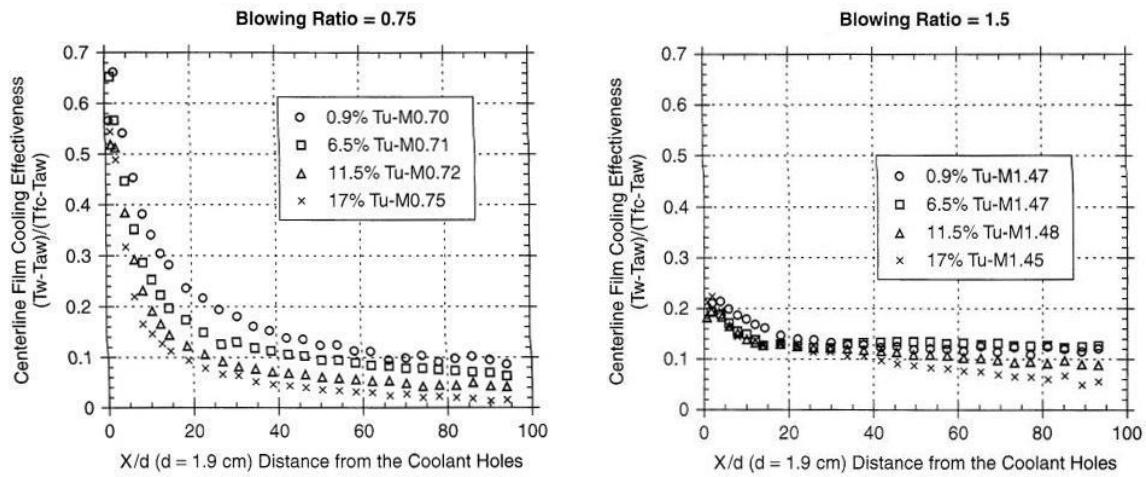


Figure 2.6: Effect of freestream turbulence on the centreline adiabatic effectiveness, [Bons et al (1996)]

2.3.7 Partial Hole Blockage

When the film cooling holes are first used they are typically clear of all unwanted debris or obstructions. However flow conditions can lead to a gradual or sudden blockage/obstruction of the film cooling holes resulting in a reduction of the film effectiveness (Fig 2.7).



Figure 2.7: Micrograph showing deposits of foreign material in a film cooling hole, [Bogard et al (1998)]

Whilst the results may seem intuitive, Bunker R.S.(2000) conducted the study due to a lack of previous work in detailing the possible reductions in film cooling efficiency due to partial blockages. Results for the adiabatic effectiveness were compared for coolant holes with no blockage, and those with partial blockage. For an exit area blockage of approximately 15% there was an almost consistent 30% decrease in the adiabatic effectiveness directly downstream of the coolant jet, with the effect becoming less pronounced as the distance from the point of injection was increased.

2.4 REVIEWS ON EFFECT OF RIBS IN INTERNAL COOLING

The purpose of introducing repeated ribs in a duct is to enhance the heat transfer rate. Ribs are man made protrusions which are placed in a controlled way along specific walls, contrary to sand-grain roughened walls, where the surface topology is stochastically distributed throughout the duct. The enhancement of the heat transfer has thus a drawback in the increased pressure drop, which can be several times higher than for a smooth channel.

The pressure drop, and also the heat transfer is strongly connected to the size of the rib, e , which is measured as a fraction of the channel height as e/H . Equivalently to the rib-height one may chose to refer to the blockage ratio, which in contemporary turbine blades are around 10-20%. Ribs have traditionally been arranged orthogonally to the flow, i.e. that the extension of the rib is located 90° to the streamwise direction.

They have commonly been made of a square cross-sectional area. Investigations J.C Han et al. (1988) have however shown that both other shapes and non-normal arranged ribs may be more beneficial to maximize the heat transfer rate. The distance between two successive ribs, the pitch P , have also been shown to be of importance, R.L. Webb et al. (1971). Thus there are a number of different parameters which could be altered in order to optimize the internal cooling of a gas turbine blade. In addition it should be noted that the available pressure difference is severely limited and hence the design of rib-roughened channels is a meticulous work, which naturally benefits from a long tradition of constructing operational gas turbine engines.

Apparent from the above discussion is that the flow pattern around the rib, varies dependent on the shape and size of the rib. In addition the distance between two consecutive ribs, the pitch P is also of importance. In experiments on rib-roughened channels, the two most significant parameters, apart from the Reynolds number, Re , are the dimensionless geometry defining ratios: the rib-height to channel-height, e/H and the rib-pitch to rib-height, P/e . The rib-width, although important for the flow structure is less

in fluently on the heat transfer it should also be pointed out that most rib-roughened channel have ribs of fairly squared cross-section.

Webb et al. (1971) compiled a number of experimental investigations to characterize the flow pattern within the interval of two success ribs for repeatedly rib-roughened channels, see Fig. 2.8. It was concluded that when the ribs are positioned far enough from each other, $P/e > 15$, the flow behaves as for a single mounted obstacle with a large re-circulating zone behind the rib, stretching roughly 6 to 8 rib-heights downstream the rib. If the pitch is smaller, the two recirculating zones (upstream and downstream the rib) start to interact. Until $P/e \approx 8$ there is still two reverse flow regions in the rib-interval, however for $P/e < 8$ the flow does not re-attaches on the channel floor between the ribs and instead a single large re-circulating bubble is created. Recently Mohamed Fathelrahman (2009) has simulated the annular flow cooling by ribbing. He has gained results demonstrating Webb experimental results on the flow structure behind the ribs.

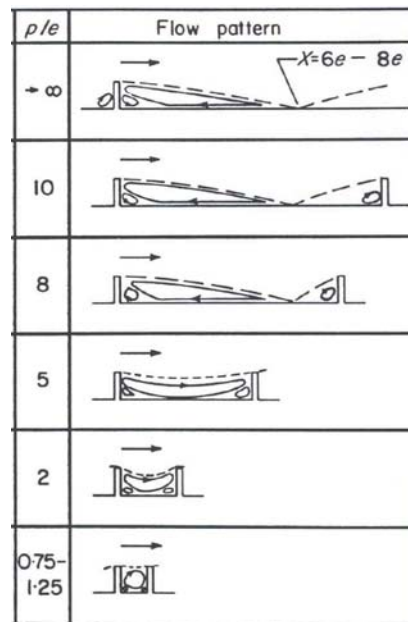


Figure 2.8: Flow patterns as a function of P/e , from [Webb et al. (1971)]

For even smaller rib-pitches the flow forms driven cavities, with a significant different heat transfer behavior. It has been shown that the most advantageous flow behavior, for heat transfer purposes, is when the flow re-attaches in-between the ribs, without re-

developing before separating due to the blockage effect of the next rib. The influence the Reynolds number, the shape and rib arrangement have on the flow structure, should however be recognized.

Liou and Hwang (1992) found for the rib-roughened flow that the Nusselt number and the turbulent kinetic energy are well correlated in the separated region behind a rib. The peak of Nusselt number was for this configuration, located around one rib-height upstream of the re-attachment point.

Investigations on angled ribs, e.g. J.C Han (1988) have showed that there is a substantial benefit of positioning the ribs with an angle to the streamwise direction as such an arrangement could achieve increase in heat transfer as compared to normal ribs. This effect may be attributed to the change in flow structure, as skewed ribs produce a secondary motion that flows transversally along the rib due to the induced cross-stream pressure gradient. A similar pattern is not found for orthogonally arranged ribs. A much weaker secondary flow with downward motion (towards the rib) along the centerline and upward along the side-wall in a circulating fashion is however present. This motion is a result of both a difference in the static pressure, and turbulent generating processes.

Please refer to section 4.3 of this report for governing equations

2.5. EFFECTS OF ROTATION ON COOLANT PASSAGE HEAT TRANSFER

The following topics will discuss the effect of rotation on coolant passage heat transfer.

2.5.1 Rotational Effect on Internal Cooling

Rotation induces Coriolis and centrifugal forces that produce cross-stream secondary flow in the rotating coolant passages; therefore, heat transfer coefficients in rotor coolant passages are very much different from those in non rotating frames. Figure 2.9 shows the schematic secondary flow and axial flow distribution in a rotating two-pass square

channel. Figure 2.10 shows the predicted secondary flow, axial flow, and temperature distribution in a rotating square channel with radial outward flow. One important finding from recent studies is that rotation can greatly enhance heat transfer on one side of the cooling channel and reduce heat transfer on the opposite side of the cooling channel due to rotating-induced secondary flow, depending on the radial outflow or inflow of the cooling passages. Without considering rotational effect, the coolant passage would be over-cooled on one side while over-heated on the opposite side. Recent studies focus on the combined effects of rotation, channel shape, orientation, and aspect ratio on rotor coolant passage heat transfer with various high performance rib turbulators. Results show that the channel shape, orientation, and aspect ratio significantly change local heat transfer coefficient distributions in rotor coolant passages with rib turbulators.

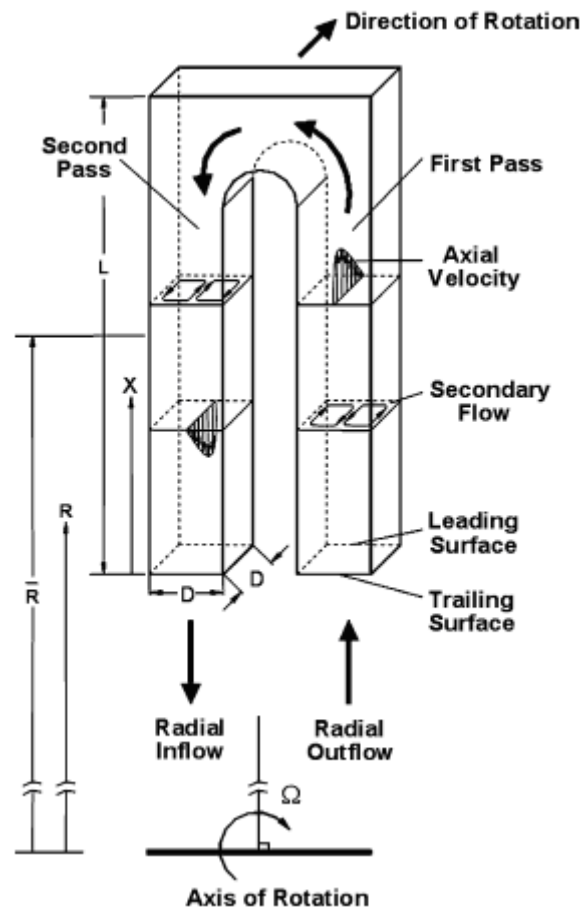


Figure 2.9: Conceptual view of a two-pass rotating coolant flow distribution by [Han et al. (1993)].

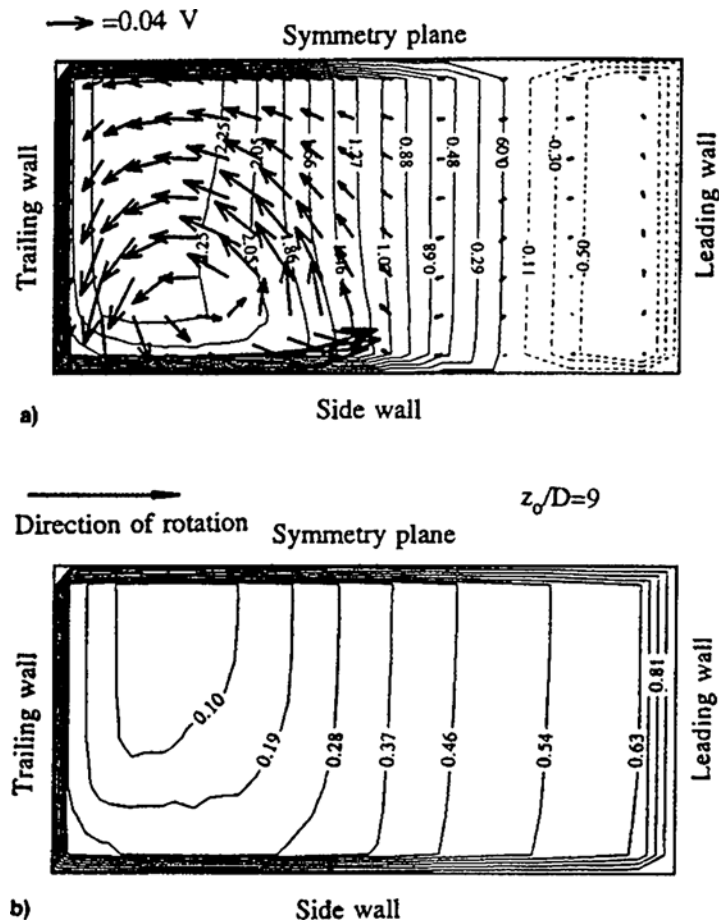


Figure 2.10: Predicted secondary flow, axial flow, and temperature distribution in a rotating square channel with radial outward flow, collected in [Han et al. (2000).]

2.5.2 Heat Transfer in Rotating Coolant Passages with Square Cross Section

Heat transfer in rotating multi-pass coolant passages with square cross section and smooth walls was reported by Wagner et al. (1991). Results show that the heat transfer coefficient can enhance 2–3 times on the trailing surface and reduce up to 50% on the leading surface for the first-pass radial outward flow passage; however, the reverse is true for the second-pass radial inward flow passage due to the flow direction change. Results also show that the heat transfer difference between leading and trailing surfaces is greater in the first-pass than that in the second pass due to the centrifugal buoyancy opposite to the flow direction. Heat transfer in rotating multi-pass coolant passages with square cross-section with 45° rib turbulated walls, as shown in Figure 2.11, was reported by Johnson et al. (1994). Results show that rotation and buoyancy, in general, have less effect on the rib turbulated coolant passage than on the smooth-wall coolant passage. This

is because the heat transfer enhancement in the ribbed passages is already up to 3.5 times higher than in the smooth passages; therefore, the rotational effect is still important but with a reduced percentage. Results also show that, like a non rotating channel, the 45° ribs perform better than 90° ribs and subsequently better than the smooth channel.

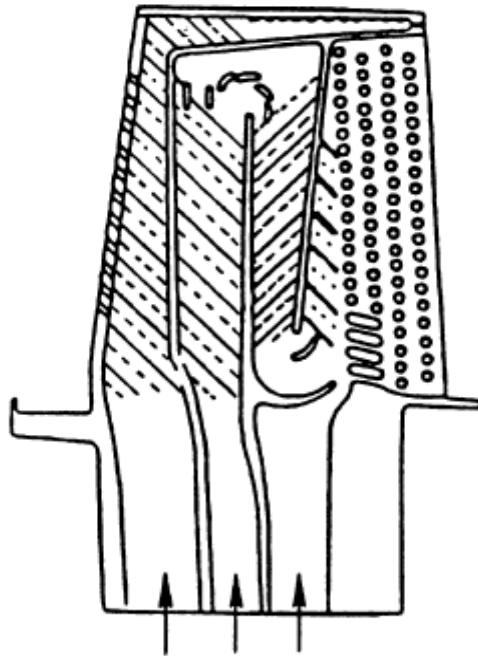
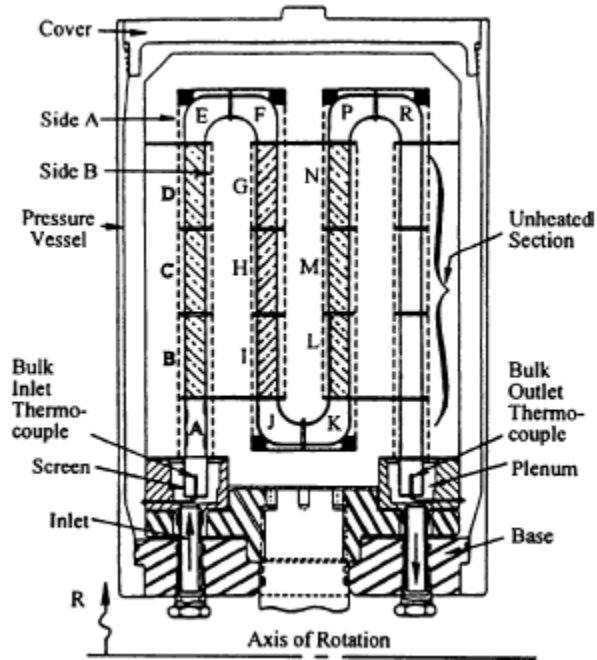


Figure 2.11: Multipass rotating channel with 45° ribs used by [Johnson et al. (1994)] to simulate a turbine rotor blade coolant passage.

2.5.3 Wall Heating Condition Effect on Rotating Coolant Passage Heat Transfer

From the above analyses, the rotation effect on channel heat transfer comes from the Coriolis and centrifugal forces. The centrifugal force is known as rotation buoyancy when there is a temperature difference between the coolant and the channel walls at rotating conditions. Since the temperature difference between the coolant and the channel walls varies along the coolant passages, so does the rotation buoyancy. Therefore, it is expected that the channel wall heating conditions would affect rotor coolant passage heat transfer. The channel heating conditions imply that the channel walls may be at the same temperature (or heat flux) in both stream-wise and circumferential coefficients on both leading and trailing surfaces. Parsons et al. (1994) studied the influence of wall heating condition on the local heat transfer coefficient in rotating two-pass square channels with 90° ribs and 60° ribs on the leading and trailing walls, respectively. They concluded that the uneven wall temperature significantly enhances heat transfer coefficients on the first-pass leading and second-pass trailing surfaces as compared with the uniform wall temperature condition.

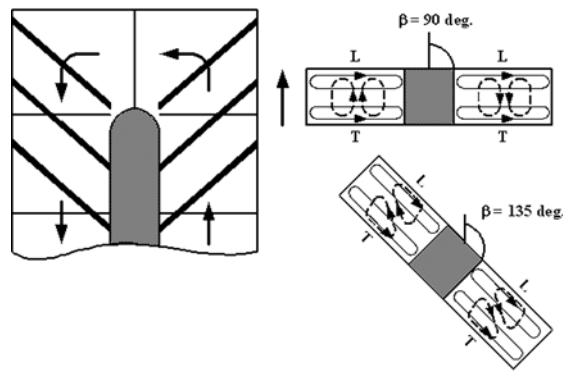
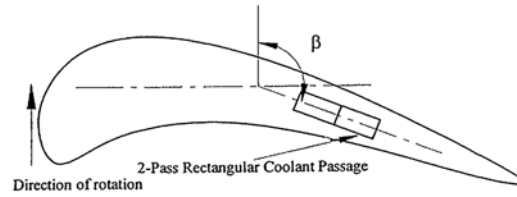
2.5.4. Heat Transfer in Rotating Coolant Passages with Rectangular Cross Section

Most of the above-mentioned studies dealt with square channels. However, a rectangular coolant passage is of high importance in order to maintain the integrity of gas turbine blade internal cooling design. The curved shape of the turbine blade may prohibit the efficient use of square cross-sectional coolant flow channels. It is quite common to find rectangular cooling passages, particularly moving from the mid-chord to the trailing edge of the blade; the channels must become more rectangular as the blade becomes thinner. This thinning of the channel changes the effective secondary flow pattern from that of a square duct. For this reason, one cannot simply apply the knowledge of the rotationally induced flow pattern and the associated surface heat transfer coefficients in a square channel to that of a rectangular channel. However, very few experimental heat transfer data on a rectangular coolant passage are available in the literature. Azad et al. (2001)

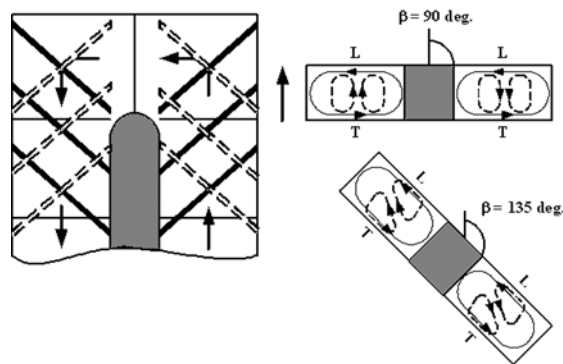
and studied heat transfer in a two-pass rectangular rotating channel (aspect ratio= 2:1) with 45° angled ribbed walls and 45° V-shaped ribbed walls, respectively, including the effect of channel orientation with respect to the axis of rotation. Figure 2.12 shows the two cell vortices induced by rotation, the two cell vortices induced by the 45° parallel ribs, and the single cell vortex induced by the 45° crossed ribs. Figure 2.13 shows the two cell vortices induced by rotation, the four cell vortices induced by 45° V-shaped ribs, and the two cell vortices induced by 45° crossed V-shaped ribs. They found that the effect of rotation on the two-pass rectangular channel is very similar to that on the two-pass square channel except the leading surface heat transfer coefficient does not vary much with the rotation compared with the square channel case. The results show that 45° parallel angled ribs produce a better heat-transfer augmentation than 45° crossed ribs; 45° V-shaped ribs are better than 45° crossed V-shaped ribs and subsequently better than 45° parallel angled ribs. The difference in heat transfer coefficients between leading and trailing surfaces in a smooth channel is smaller when the channel has an angle with respect to the axis of rotation. This heat transfer coefficient difference is reduced further in ribbed channel cases. Griffith et al. (2001) studied heat transfer in a single pass rectangular channel (aspect ratio=4:1) with smooth and 45° angled ribbed walls, as shown in Figure 2.14, including the effect of channel orientation with respect to the axis of rotation. Results show that the narrow rectangular passage exhibits a much higher heat transfer enhancement for the ribbed surface than the square and 2:1 channels previously investigated. Also, channel orientation significantly affects the leading and side surfaces, yet does not have much affect on the trailing surfaces for both smooth and ribbed surfaces. Therefore, this investigation has determined that span-wise variations in the heat transfer distribution of rectangular cooling passages exist, and that the enhancement is a function of channel orientation with respect to the axis of rotation, surface configuration (such as smooth or 45° angled ribbed walls), and channel aspect ratio.

Willett and Bergles (2000) studied heat transfer in a single pass narrow, 10:1 smooth rectangular channel oriented at an angle to the axis of rotation. They focused on the rotating buoyancy effect on local heat transfer coefficients. They found that the channel orientation induced a significant variation in the heat transfer coefficient in the span-wise

direction. They also found that the heat transfer coefficient at the far aft end of the trailing surface is a very strong function of rotation buoyancy.

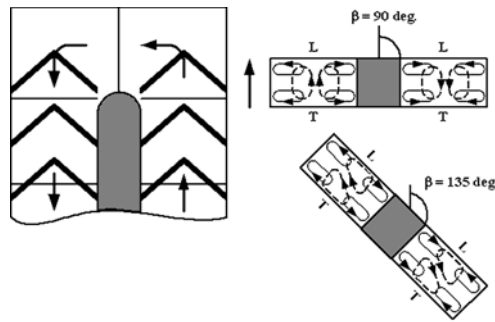


Parallel 45 Deg. Angled Ribs

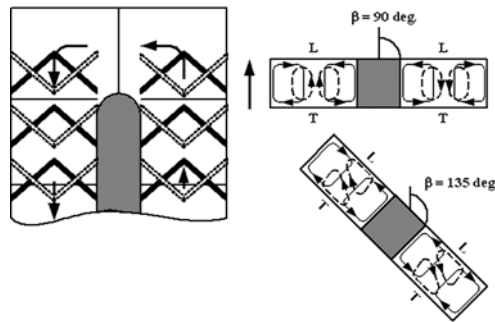


Crossed 45 Deg. Angled Ribs

Figure 2.12: Conceptual view of the secondary flow vortices induced by rotation and channel orientation in a two-pass rectangular channel (dash lines: rotation-induced vortices; solid lines: rib-induced vortices) from [Azad et al. (2001).]



Parallel 45 Deg. V-shaped Ribs



Crossed 45 Deg. V-shaped Ribs

Figure 2.13: Conceptual view of the secondary flow vortices induced by rotation and channel orientation in a two-pass rectangular channel (dash lines: rotation-induced vortices; solid lines: rib-induced vortices) from [Al-Hadhrami et al. (2002)].

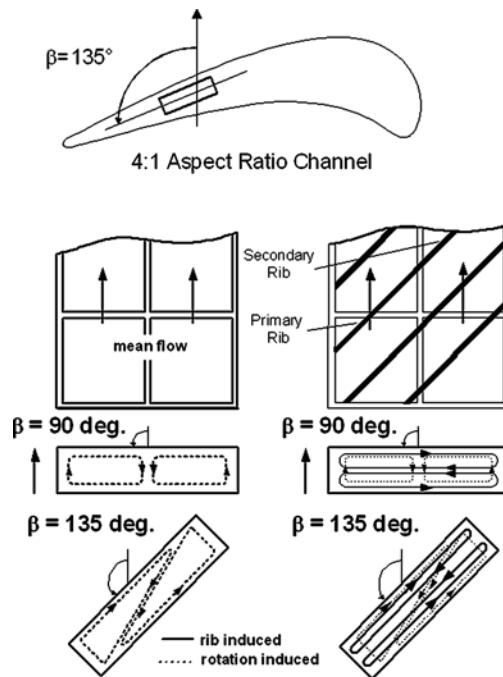


Figure 2.14: Outward flow rectangular test section with smooth walls and 45° parallel angled ribs on leading and trailing surfaces by [Griffith et al. (2001)].

CHAPTER 3

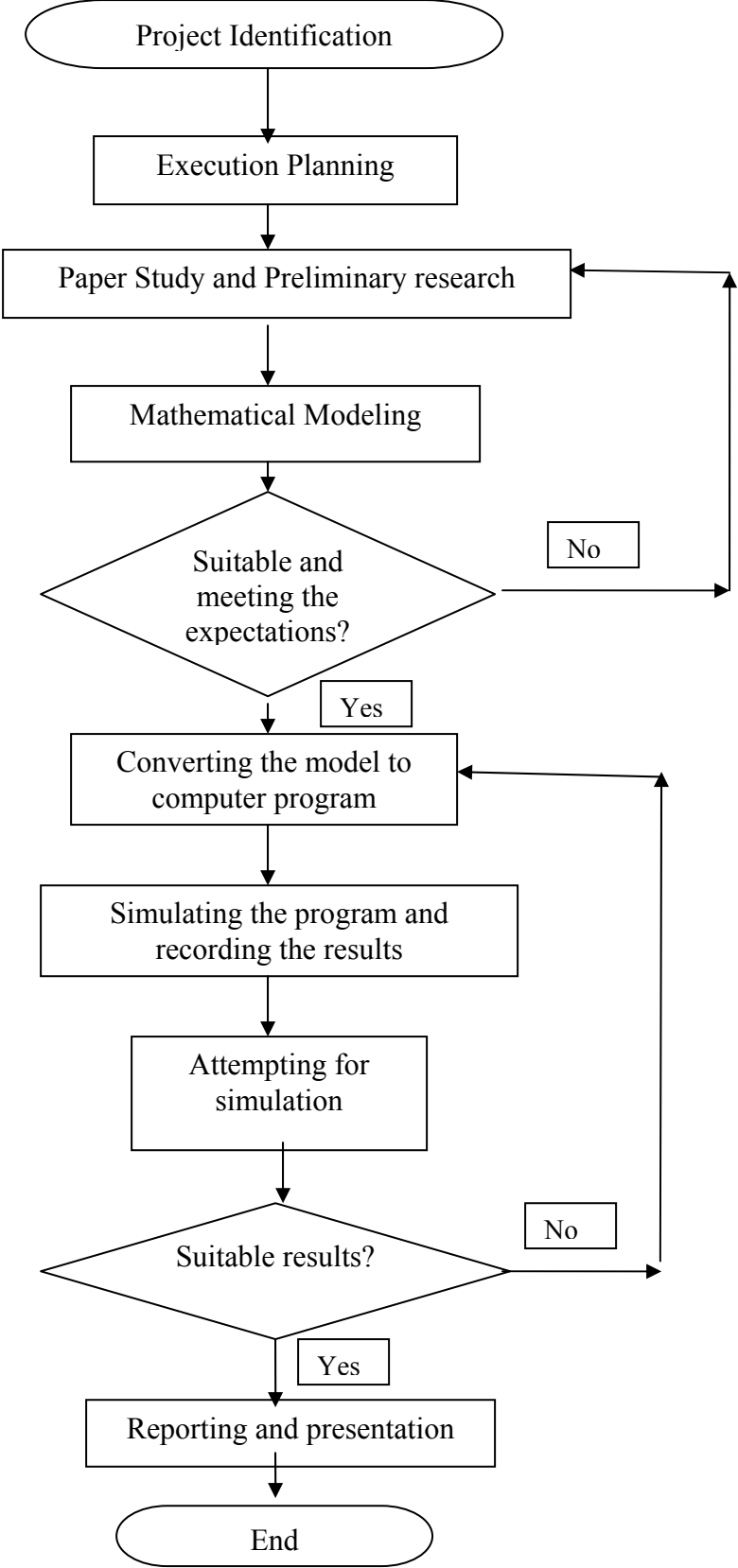
METHODOLOGY

This chapter covers the analysis techniques, the project execution flow chart and Gantt chart for FYP II.

3.1 ANALYSIS TECHNIQUES

Project consists information gathering on cooling system of Gas Turbines as a literature review. After getting familiar with gas turbine cooling system, the flow of hot gases and compressed air inside the gas turbine is modeled with the help of heat transfer and fluid dynamic relations. Heat transfer and flow dynamic correlations in smooth and ribbed channels are selected. Blade profile is determined by CNC Laser Digitizer. The profile is then converted to Auto CAD drawing to mesh the model. The mathematical model is converted to a computer program to perform simulation in different operating conditions. The Finite-Difference approach is adopted and the matrix of the nodal equations is solved by MATLAB and Excel. Analyses are done under various operation conditions for smooth and ribbed channels. Conclusion and recommendations are made according to the obtain results.

3.2 WORK FLOW CHART



3.3 GANTT CHART

Table 3-1: FYP II Gantt chart

Detail of Activities	Week															
	1	2	3	4	5	6	7	8	9		10	11	12	13	14	
MATLAB and Excel programming	■	■								Mid Semester Break						
work on h , Nu and Re relations		■	■	■	■											
Submission of Progress Report				■												
Literature and paper review	■	■	■	■	■	■	■	■	■			■	■	■	■	■
Study on ribbed channels and calculation						■	■	■	■			■	■	■		
Progress report submission								■								
Seminar								■								
Poster Presentation												■				
Submission of Dissertation(softcopy)														■		
Oral Presentation																■
Dissertation Submission(hardcopy)																7 days after presnt.

Study Week

CHAPTER 4

PREPARATIONS AND DISCUSSION OF RESULTS

A gas turbine blade was chosen from building 18 to be modeled in computer (Look at figure 4.1). The cross section of the blade as well as location and dimensions of the internal air channel were modeled in Auto Cad software as a 3-D object. The blade cross section on the leading edge of the model was meshed and the irregularities were approximated. Meshing resulted in 82 nodes on the cross section of the blade (look at Fig.4.2).

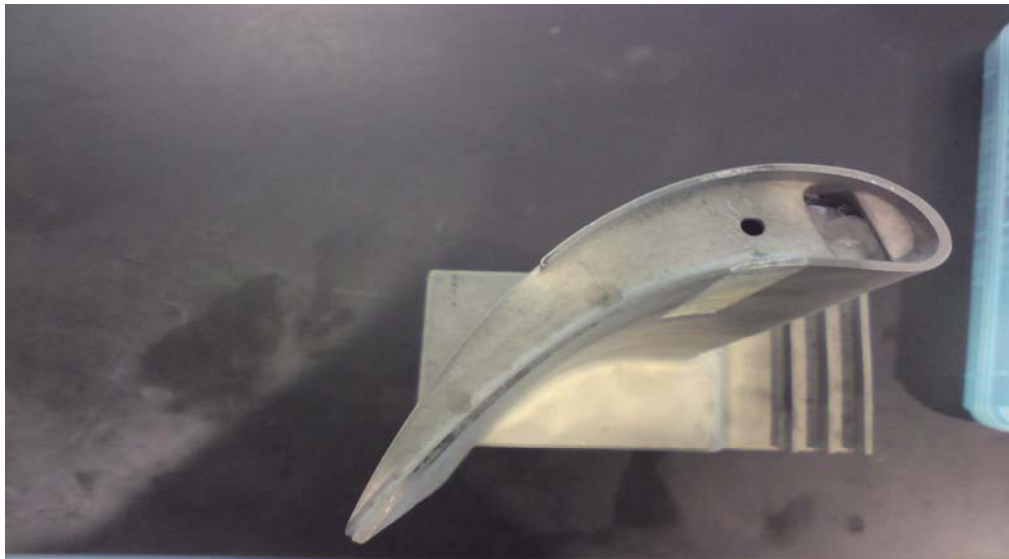


Figure 4.1: GT blade in building 18

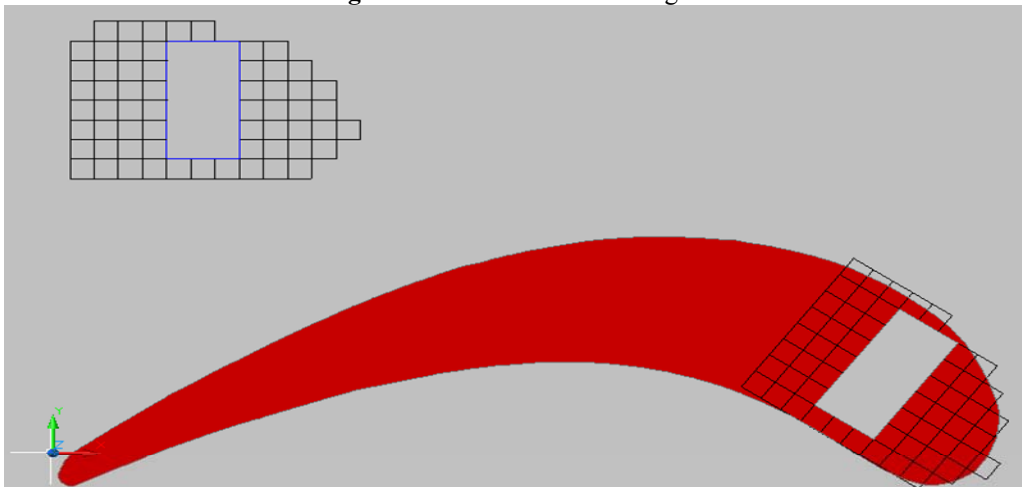


Figure 4.2: Cross-section of the modeled GT blade and correspondence meshing around the internal air channel

The 3-D model is shown in Fig 4.3 as follow:

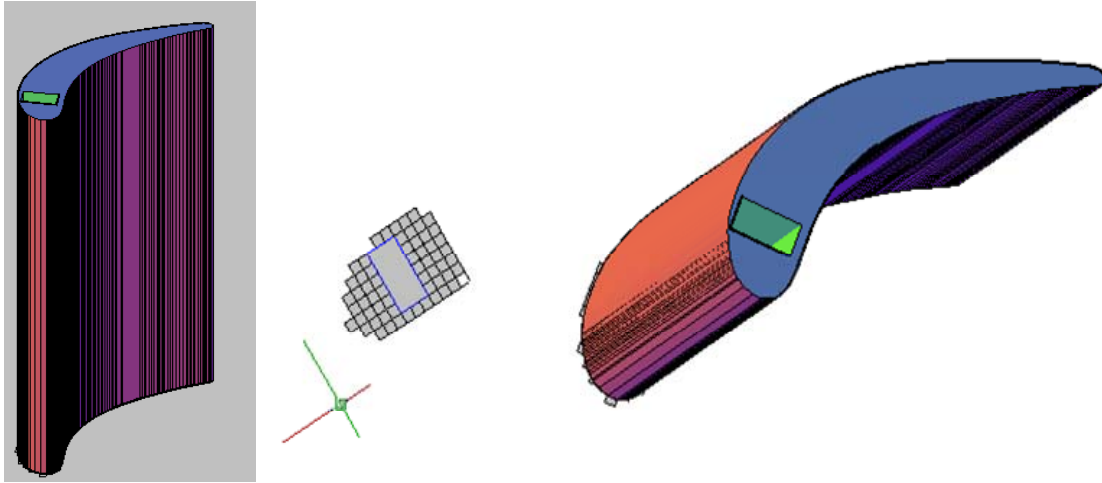


Figure 4.3: 3-D model of the blade

4.1 NODAL EQUATIONS

The nodal equations used in this work are given in this section.

Energy equation based on conservation of energy can be written is as follow:

$$q_{in} - q_{out} + q_{generated} = q_{stored} \quad (4-a)$$

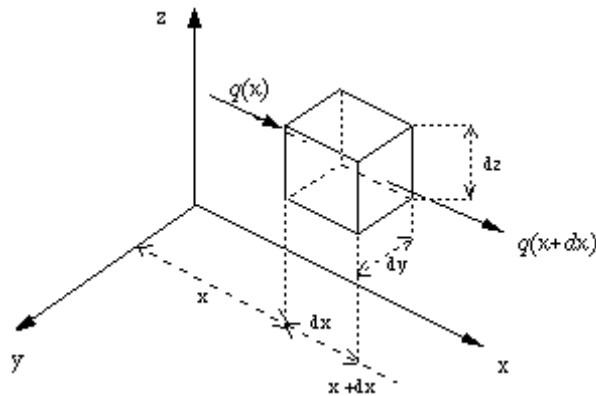


Figure 4.4: Heat transfer in an infinitesimal small control volume

Consider an infinitesimally small control volume dx, dy, dz and apply the energy balance we have:

$$\frac{\partial}{\partial x}\left(k \frac{\partial T}{\partial x}\right) + \frac{\partial}{\partial y}\left(k \frac{\partial T}{\partial y}\right) + \frac{\partial}{\partial z}\left(k \frac{\partial T}{\partial z}\right) + \dot{q} = \rho c_p \frac{\partial T}{\partial t} \quad (4-b)$$

Considering steady state condition ($\frac{\partial T}{\partial t}=0$) and no heat generation ($\dot{q}=0$) for 2-D case

we get the *general heat transfer equation* which is:

$$\frac{\partial^2 T}{\partial x^2} + \frac{\partial^2 T}{\partial y^2} = 0 \quad (4-c)$$

Temperature analysis was performed on the nodes using Finite-D method. Heat transfer equations for convection and conduction were widely used to solve the problem. By adopting the energy balance on the node of interest based on the general thermal situation shown in Fig 4.5, following equation can be written:

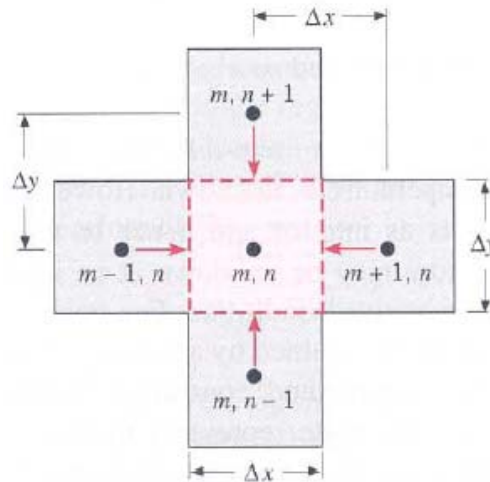
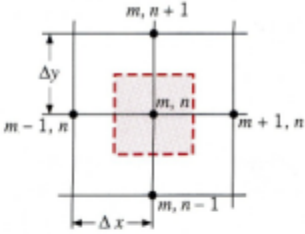
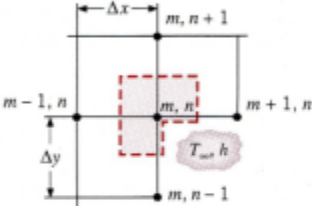
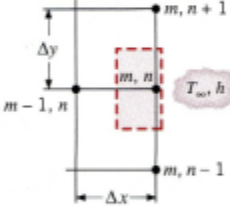
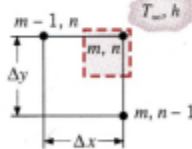
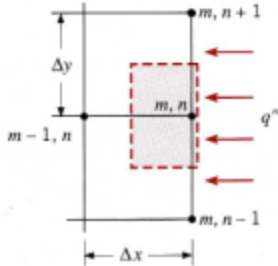


Figure 4.5: Conduction to an interior node from its adjoining nodes (Dewill et al., 2007)

$$Q_1 + Q_2 + Q_3 + Q_4 + Q_g = Q_{\text{stored}} \quad (\text{Energy conservation}) \quad (4-d)$$

For the blade cooling case, there is no heat generation, $Q_g=0$, and for steady state condition $Q_{\text{stored}}=0$. This will lead to $Q_1 + Q_2 + Q_3 + Q_4 = 0$, possible nodal thermal modes are presented in Table 4.1.

Table 4-1: Summary of nodal finite-difference equations (Dewill et al., 2007)

Configuration	Finite-Difference Equation for $\Delta x = \Delta y$
	$T_{m,n+1} + T_{m,n-1} + T_{m+1,n} + T_{m-1,n} - 4T_{m,n} = 0$ <p>Case 1. Interior node</p>
	$2(T_{m-1,n} + T_{m,n+1}) + (T_{m+1,n} + T_{m,n-1}) + 2\frac{h\Delta x}{k}T_{\infty} - 2\left(3 + \frac{h\Delta x}{k}\right)T_{m,n} = 0$ <p>Case 2. Node at an internal corner with convection</p>
	$(2T_{m-1,n} + T_{m,n+1} + T_{m,n-1}) + \frac{2h\Delta x}{k}T_{\infty} - 2\left(\frac{h\Delta x}{k} + 2\right)T_{m,n} = 0$ <p>Case 3. Node at a plane surface with convection</p>
	$(T_{m,n-1} + T_{m-1,n}) + 2\frac{h\Delta x}{k}T_{\infty} - 2\left(\frac{h\Delta x}{k} + 1\right)T_{m,n} = 0$ <p>Case 4. Node at an external corner with convection</p>
	$(2T_{m-1,n} + T_{m,n+1} + T_{m,n-1}) + \frac{2q''\Delta x}{k} - 4T_{m,n} = 0$ <p>Case 5. Node at a plane surface with uniform heat flux</p>

Please refer to section 4.3 of this report for ribbed channels' specific correlations and formulas.

4.2 RESULTS FOR SMOOTH CHANNEL

Using the nodal equations, one equation was written for every node the result is 82 equations with 82 unknowns (Temperature for every node) to be solved. Microsoft excel was programmed to prepare the coefficient and known matrix for the condition specified by the user. Results presented here are based on the following information:

- Temperature of hot gas (T_o) attacking the blade is 1700 K
- Temperature of compressed air (T_i) entering the channel is 400 K
- Convection heat transfer coefficient (h_o) for the hot gas is $1000 \text{ W/m}^2 \cdot \text{K}$
- For the meshing $\Delta x = 3 \text{ mm}$
- The size of the air channel and the height of the blade are 9mm x 18mm and 21 cm respectively ($a=18 \text{ mm}$, $b=9 \text{ mm}$)
- An adiabatic wall is assumed to exist on the left hand side where the meshing is terminated (Look at Fig 4.6, nodes : $T_1, T_7, T_{16}, T_{24}, T_{33}, T_{42}, T_{52}, T_{62}, T_{73}$ are located on adiabatic wall). These nodes belong to case 5 of table 4.1 when q'' is equal to zero.
- Mass flow rate of compressed air entering the channel is 0.01 kg/s.

In order to find temperature distribution around the leading edge, convection heat transfer coefficient (h_i) for the air should be calculated first.

For a smooth rectangular channel, *Reynolds number* can be evaluated using hydraulic

diameter D_h , where $D_h = \frac{4A_c}{P}$ (A_c and $P = 2(a + b)$ are the flow cross section area and the

wetted parameter respectively). $Re_{D_h} = \frac{u_m \rho D_h}{\mu}$ and $u_m = \frac{\dot{m}}{\rho A_c}$. Substituting D_h and u_m in

Re_D we have $Re_{D_h} = \frac{4\dot{m}}{P\mu}$ ($\mu = 230.1 \times 10^{-7} \text{ N.s/m}^2$ at 400 K and $P = 0.054 \text{ m}$)

Substituting the respective values, $Re_{D_h} = 32192.12$, so the flow inside the channel will be turbulent.

For a turbulent flow that is fully developed Nu number can be calculated using *Dittus-Boelter equation* where $Nu = 0.023 Re^{4/5} Pr^n$. Air is heated inside the channel so $n=0.4$, taking $Pr \approx 0.7$ at 400 K, $Nu=79.60$.

Finally h_i can be calculated using $h_i = \frac{Nuk_{air}}{D_h}$

Air is entering the channel at 400 K so $k_{air} = 33.8 \times 10^{-3} W/m.k$, substituting all the values in above equation $h_i = 224.22 W/ m^2 .k$

Now temperature distribution in blade cross section at the root can be evaluated as shown in Fig. 4.6.

T1	T2	T3	T4	T5	T6						
1502.36	1500.89	1497.34	1495.39	1506.03	1523.56						
T7	T8	T9	T10	T11	T12	T13	T14	T15			
1480.12	1478.03	1472.21	1464.55	1479.32	1498.73	1541.31	1567.06	1585.82			
T16	T17	T18	T19			T20	T21	T22	T23		
1462.07	1458.89	1448.94	1430.04			1527.22	1554.60	1577.17	1596.81		
T24	T25	T26	T27			T28	T29	T30	T31	T32	
1450.36	1446.54	1434.62	1413.17			1519.04	1546.95	1570.86	1591.68	1608.97	
T33	T34	T35	T36			T37	T38	T39	T40	T41	
1446.30	1442.28	1429.83	1407.91			1515.23	1543.32	1567.63	1588.30	1604.41	
T42	T43	T44	T45			T46	T47	T48	T49	T50	T51
1450.27	1446.44	1434.51	1413.05			1515.26	1543.47	1568.03	1589.48	1609.12	1627.22
T52	T53	T54	T55			T56	T57	T58	T59	T60	T61
1461.90	1458.71	1448.72	1429.78			1518.89	1547.27	1571.55	1592.46	1611.16	1627.85
T62	T63	T64	T65	T66	T67	T68	T69	T70	T71	T72	
1479.90	1477.79	1471.89	1464.05	1478.32	1497.21	1525.98	1555.18	1578.43	1597.65	1614.65	
T73	T74	T75	T76	T77	T78	T79	T80	T81	T82		
1502.14	1500.64	1496.99	1494.84	1505.02	1521.80	1545.00	1569.03	1589.34	1604.90		

Figure 4.6: Temperature (K) distribution in the cross section of GT blade surrounding the cooling passage at root of the blade.

Air temperature continuously changes when flowing in the channel this in turn changes temperature distribution for every cross section one may choose along the height. In this discussion the blade is divided to four equal segments along the height and temperature distribution in each segment is discussed as follow.

The rate of heat transfer per unit length of the channel may be expressed as the following formula for the first segment (H=0 to H=5.25cm):

$$q' = h_1 [\Delta x * (T_{20} + T_{28} + T_{37} + T_{46} + T_{56} + T_{19} + T_{27} + T_{36} + T_{45} + T_{55} + T_{10} + T_{11} + T_{65} + T_{68} + T_{66} + T_{67} - 16 * T_i) + \Delta x / 2 * (T_{12} + T_{13} - 2 * T_i) + \Delta x * (T_o - T_i)] =$$

$$\mathbf{13196.71 \text{ W/m \#}}$$

Knowing the length of the first segment (5.25 cm) and for air at 400 K $C_p = 1014 \text{ J/Kg.K}$, temperature difference of compressed air across the channel can be calculated as follow:

$$q_{Total} = H_{segment} \times q'$$

$$q_{Total} = C_p \times \dot{m}_{air} \times \Delta T_{air}$$

Substituting the respective values in the above equations and assuming $\dot{m}_{air} = 0.01 \text{ Kg/s}$ we have:

$$q_{Total} = 692.83 \text{ W}$$

$$\Delta T_{air} = 68.33 \text{ K}$$

Now air is entering to the second section at 468.33 K, properties of air should be measured in this new temperature. The above calculations are repeated again. At this temperature the following properties for air are obtained:

$$C_p = 1024.30 \text{ J / kg.K}$$

$$\mu \times 10^7 = 257.81 \text{ N.s / m}^2$$

$$k_{air} \times 10^3 = 38.55 \text{ W / m.K}$$

Using the same calculations as segment one we have:

$$h_2 = 233.49 \text{ W / m}^2 .K$$

$$q_{total} = 679.11 \text{ W}$$

$$\Delta T_{air} = 66.30 \text{ K}$$

Applying h_2 temperature distribution is shown in Fig 4.7.

T1	T2	T3	T4	T5	T6						
1512.06	1510.65	1507.26	1505.37	1515.43	1532.08						
T7	T8	T9	T10	T11	T12	T13	T14	T15			
1490.91	1488.92	1483.37	1476.04	1490.00	1508.43	1548.43	1573.05	1590.97			
T16	T17	T18	T19			T20	T21	T22	T23		
1473.76	1470.74	1461.28	1443.32			1535.00	1561.16	1582.72	1601.48		
T24	T25	T26	T27			T28	T29	T30	T31	T32	
1462.63	1459.00	1447.69	1427.33			1527.21	1553.87	1576.70	1596.59	1613.10	
T33	T34	T35	T36			T37	T38	T39	T40	T41	
1458.77	1454.95	1443.14	1422.34			1523.60	1550.43	1573.63	1593.37	1608.75	
T42	T43	T44	T45			T46	T47	T48	T49	T50	T51
1462.53	1458.90	1447.57	1427.20			1523.66	1550.59	1574.03	1594.50	1613.25	1630.53
T52	T53	T54	T55			T56	T57	T58	T59	T60	T61
1473.57	1470.54	1461.04	1443.03			1527.16	1554.24	1577.41	1597.36	1615.21	1631.13
T62	T63	T64	T65	T66	T67	T68	T69	T70	T71	T72	
1490.67	1488.65	1483.02	1475.49	1488.89	1506.73	1533.99	1561.82	1583.99	1602.32	1618.54	
T73	T74	T75	T76	T77	T78	T79	T80	T81	T82		
1511.82	1510.38	1506.88	1504.76	1514.32	1530.18	1552.17	1575.05	1594.41	1609.25		

Figure 4.8 : Temperature (K) distribution in the cross section of the third segment (H=10.5 to H=15.75 cm) of GT blade surrounding the cooling passage

For the fourth segment air enters at 598.35 K, properties of air at this condition are:

$$C_p = 1050.64 J / kg.K$$

$$\mu \times 10^7 = 305.23 N.s / m^2$$

$$k_{air} \times 10^3 = 46.80 W / m.K$$

Using these values:

$$h_4 = 247.64 W / m^2.K$$

$$q_{total} = 637.92 W$$

$$\Delta T_{air} = 60.72 K$$

Applying h_4 temperature distribution is shown below:

T1	T2	T3	T4	T5	T6						
1518.73	1517.37	1514.10	1512.27	1521.95	1538.00						
T7	T8	T9	T10	T11	T12	T13	T14	T15			
1498.34	1496.42	1491.07	1483.98	1497.40	1515.17	1553.59	1577.37	1594.69			
T16	T17	T18	T19			T20	T21	T22	T23		
1481.80	1478.89	1469.77	1452.45			1540.62	1565.90	1586.72	1604.84		
T24	T25	T26	T27			T28	T29	T30	T31	T32	
1471.07	1467.57	1456.67	1437.04			1533.11	1558.86	1580.92	1600.12	1616.07	
T33	T34	T35	T36			T37	T38	T39	T40	T41	
1467.35	1463.67	1452.28	1432.24			1529.63	1555.54	1577.95	1597.02	1611.87	
T42	T43	T44	T45			T46	T47	T48	T49	T50	T51
1470.97	1467.47	1456.55	1436.91			1529.69	1555.70	1578.35	1598.12	1616.22	1632.91
T52	T53	T54	T55			T56	T57	T58	T59	T60	T61
1481.61	1478.69	1469.53	1452.16			1533.08	1559.24	1581.61	1600.88	1618.11	1633.49
T62	T63	T64	T65	T66	T67	T68	T69	T70	T71	T72	
1498.10	1496.15	1490.70	1483.43	1496.29	1513.45	1539.71	1566.57	1587.97	1605.67	1621.33	
T73	T74	T75	T76	T77	T78	T79	T80	T81	T82		
1518.49	1517.10	1513.72	1511.65	1520.83	1536.09	1557.28	1579.35	1598.03	1612.37		

Figure 4.9 : Temperature (K) distribution in the cross section of the fourth segment (H=15.75 to H=21 cm) of GT blade surrounding the cooling passage

Air finally leaves the channel at **659.07 K**.

So the total increase in air temperature will be 259 K. If we neglect the changes in air properties when passing the channel then total air temperature difference will be 273 K means air is leaving at 673 K so if constant properties is assumed for air then the error is

$$\varepsilon = \left| \frac{659 - 673}{659} \right| \times 100, \text{ which is only } 2.12\%.$$

The following graph shows air leaving temperature versus air mass flow rate assuming constant properties for air.

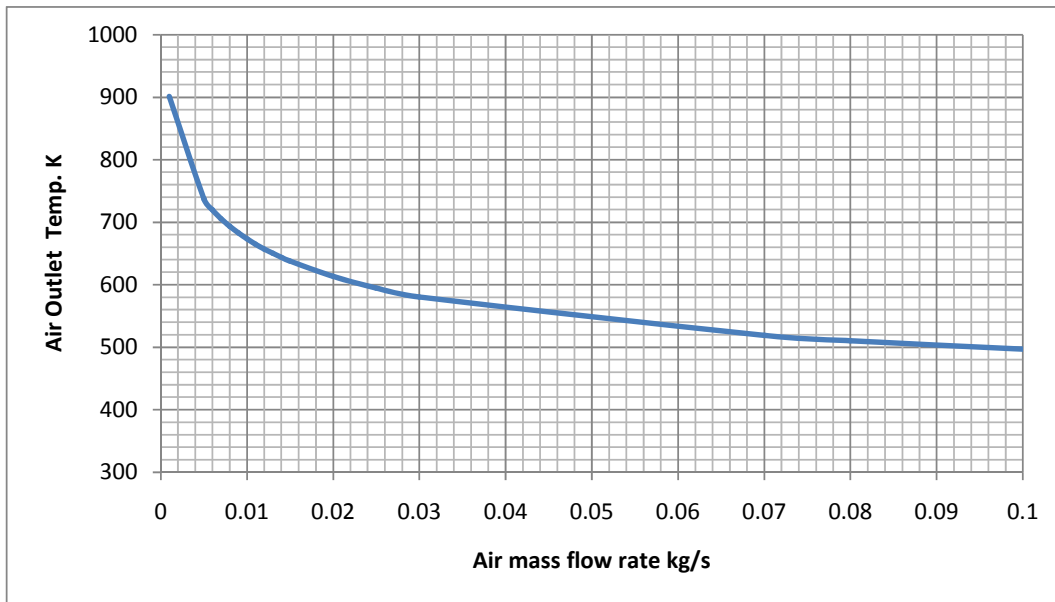


Figure 4.10 : Air outlet temperature (K) for different mass flow rates (kg/s) for smooth channel

Figure below is demonstrating air mass flow rate and convection coefficient relation.

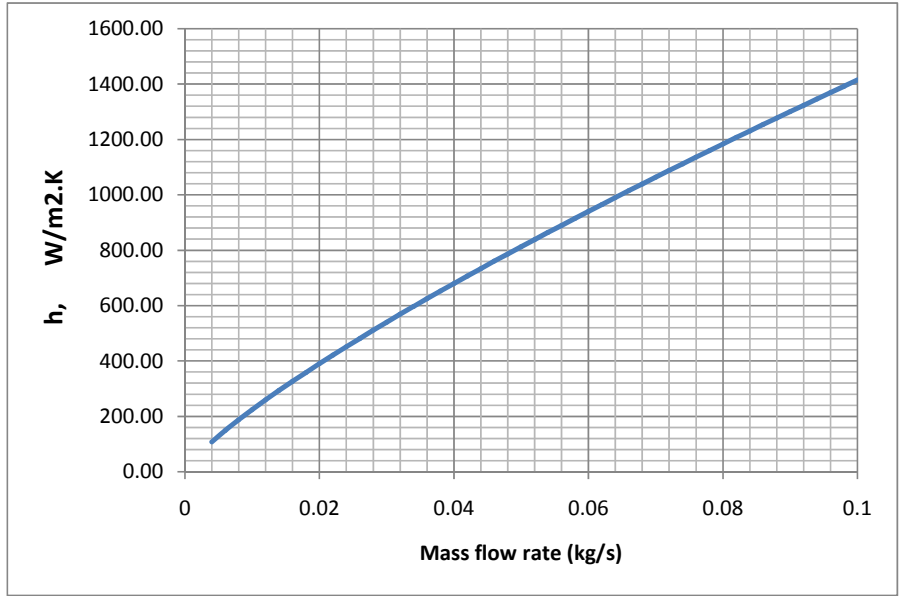


Figure 4.11 : Convection coefficient (W/m².K) for different air mass flow rates (kg/s) in smooth channel

Change in convection coefficient is shown across the channel in the following graph:

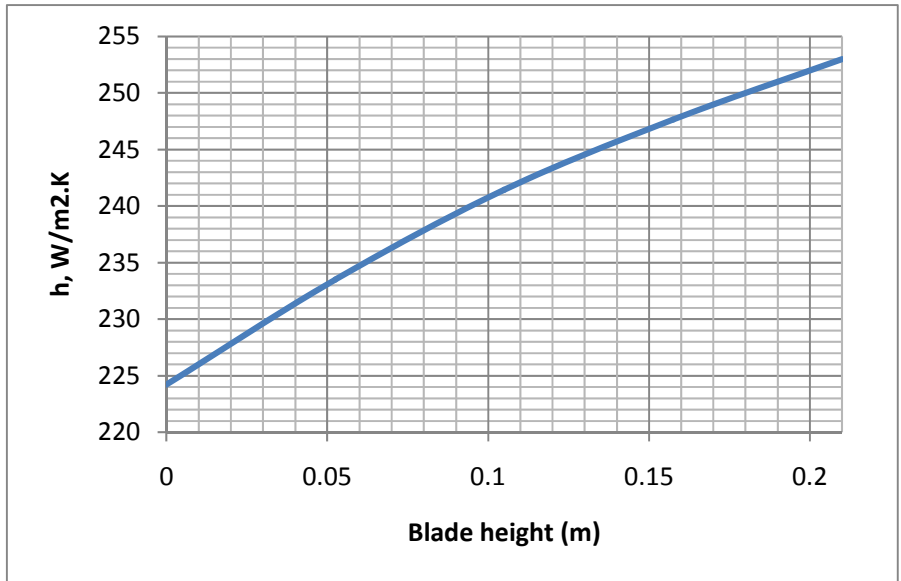


Figure 4.12 : Local convection coefficient in the smooth channel

According to Fig.4.9 the following graphs are obtained:

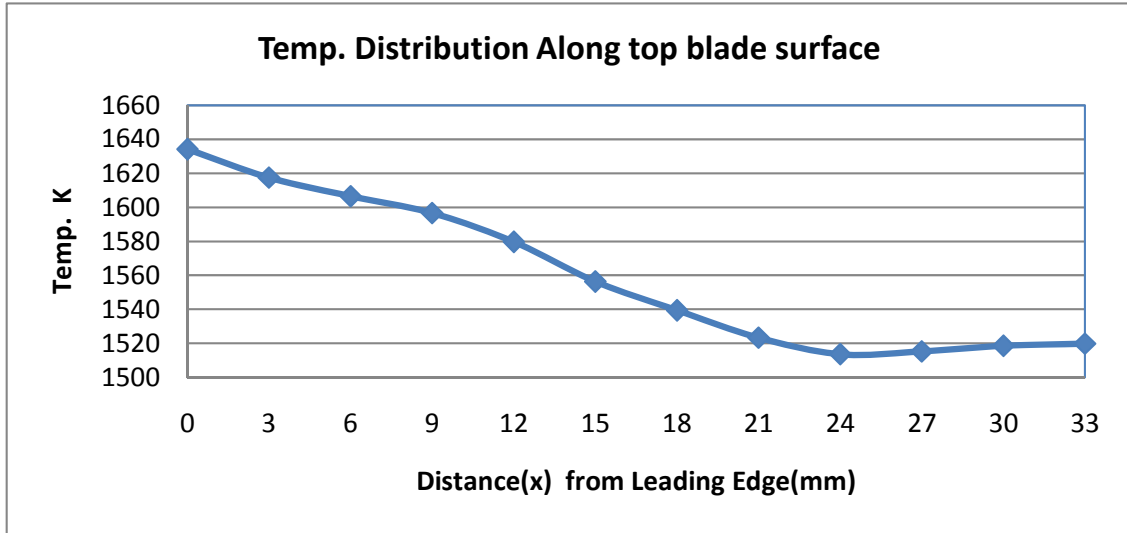


Figure 4.13 : Temperature (K) distribution along top blade surface (H=15.75 to H=21 cm).

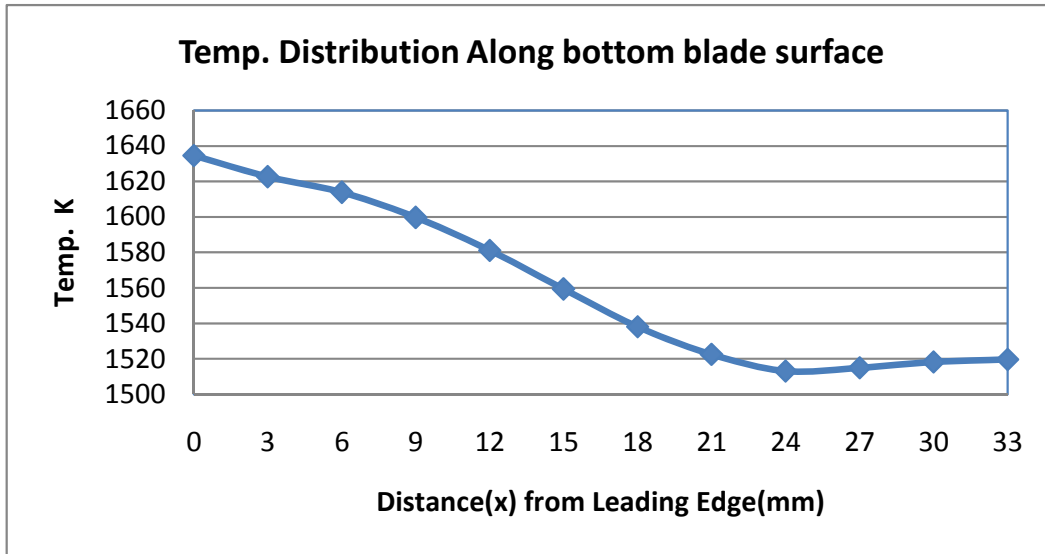


Figure 4.14: Temperature (K) distribution along bottom blade surface (H=15.75 to H=21 cm).

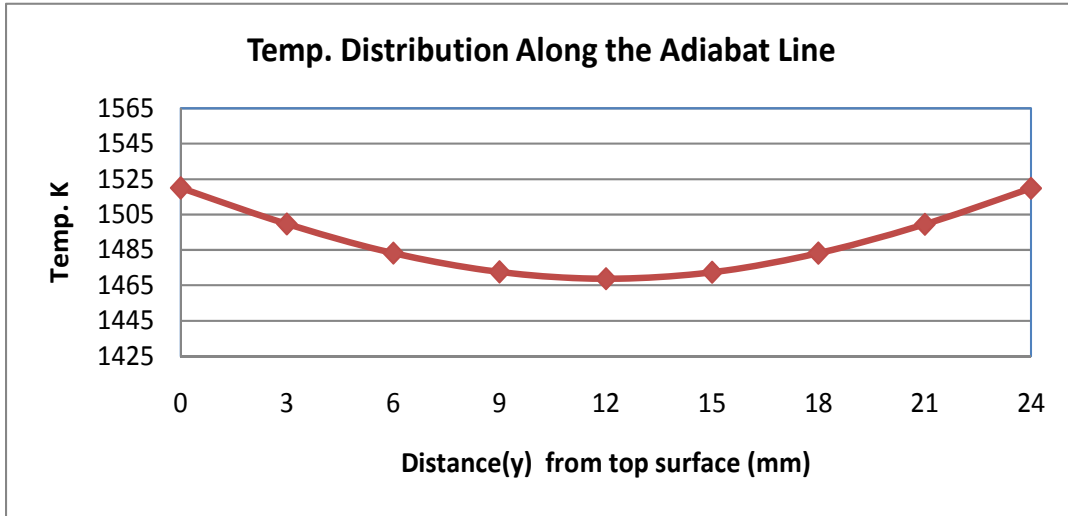


Figure 4.15 : Temperature distribution along the adiabatic line

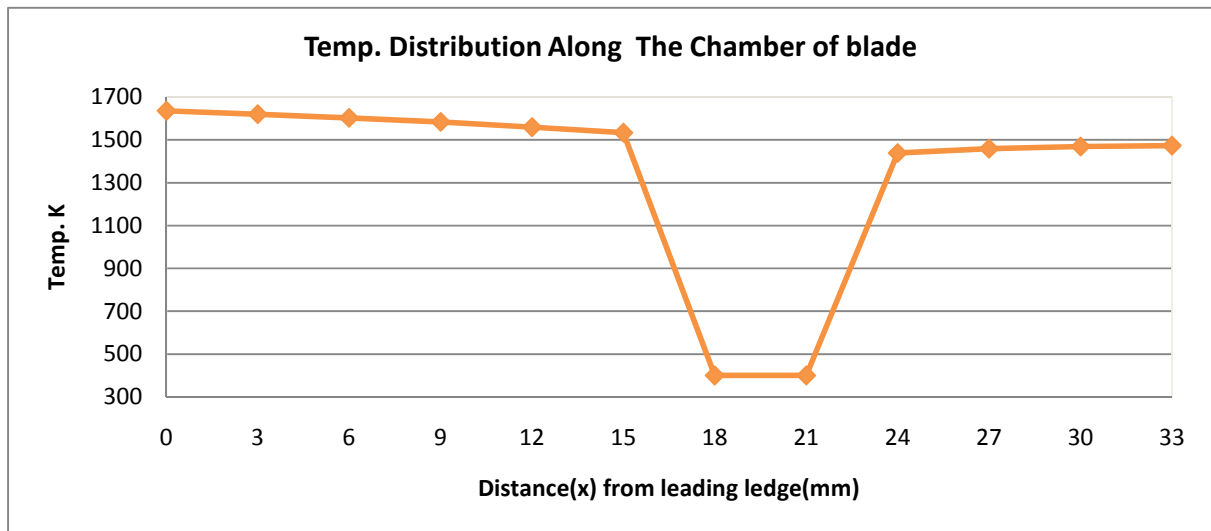


Figure 4.16 : Temperature distribution along the chamber of blade

For further discussion please refer to section 4.4, discussion on the results.

4.3. RESULTS FOR RIBBED CHANNEL

Section 4.2 was concerned about the smooth channel, in this part of the report effect of introducing rib angles, α of 90° , 60° , 45° and 30° and ribs blockage ratios, e/D_h ranging from 0.042 to 0.078 for two opposite sides of the discussed channel of compressed air will be evaluated.

One very important factor affecting the heat transfer enhancement and pressure drop inside the ribbed channel is found to be channel aspect ratio (W/H), where W is the width of the ribbed side of the channel and H is the height of the smoothed side.

According to the literature usually the suction and pressure side of the channel are ribbed so in our case $W=9$ mm and $H=18$ mm. ($W/H=1/2$)

Han (1998) developed a correlation to predict the performance of two-sided orthogonal ribbed rectangular channels. The roughness function R was given by

$$R(e^+) = \left(\frac{2}{f}\right)^{1/2} + 2.5 \ln\left(\frac{2e}{D} \frac{2W}{W+H}\right) + 2.5 \quad (4-1)$$

And the heat transfer roughness function G was given by

$$G(e^+, \text{Pr}) = R(e^+) + \frac{(f/2St_r) - 1}{(f/2)^{1/2}} \quad (4-2)$$

The roughness Reynolds number e^+ is given by

$$e^+ = (e/D) \text{Re}(f/2)^{1/2} \quad (4-3)$$

The four-sided ribbed channel friction factor f is given by

$$f = \bar{f} + (H/W)(\bar{f} - f_s) \quad (4-4)$$

- \bar{f} is average friction factor in a channel with two opposite ribbed walls
- f_s is the friction factor four smooth-sided channels
- St_r is ribbed sidewall centerline average Stanton number for flow in a channel with two opposite ribbed walls

Therefore \bar{f} and St_r for a desired operating condition (given $W/H, e/D$ and Re) can be predicted from experimentally obtained R and G correlations.

It should be noted that f_s in equation (4-4) can be obtained from Colebrook equation:

$$\frac{1}{\sqrt{f_s}} = -2.0 \log \left(\frac{\varepsilon/D}{3.7} + \frac{2.51}{Re \sqrt{f}} \right) \quad (\text{Turbulent flow}) \quad (4-5)$$

When solving the above equation with Newton iterations a good first guess can be obtained from the equation (4-6) below:

$$\frac{1}{\sqrt{f_s}} \cong -1.80 \log \left[\frac{6.9}{Re} + \left(\frac{\varepsilon/D}{3.7} \right)^{1.11} \right] \quad (4-6)$$

- ε is roughness value and D should be substituted by hydraulic diameter D_h .

Han et al., 1989 obtained the relation between G and e^+ as well as R and α in narrow – aspect ratio rectangular ribbed channels as indicated in the figure 4.17, below.

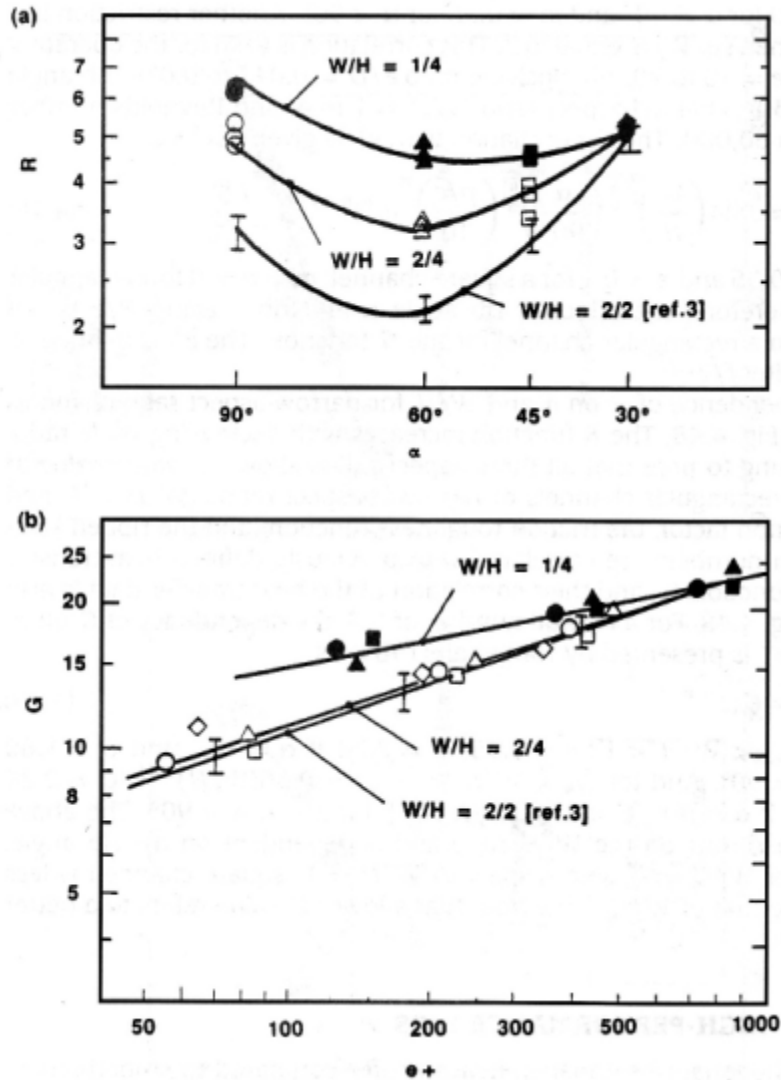


Figure 4.17: Friction factor and heat transfer correlation in narrow-aspect ratio rectangular ribbed channels (Han et al., 1989)

4.3.1 Introducing Orthogonal Ribs ($\alpha = 90^\circ$)

According to the figure 4.17 (a) above, in this case ($W/H = \frac{1}{2}$) an approximate value of 5 for R can be obtained. Using this value in equation (4-1) and substituting other values ($Re=32192.12$, $W = 9mm$, $H = 18mm$) and assuming rib blockage ratios, $e/D_h=0.063$, friction factor for four-sided ribbed channel is calculated as:

$$f = 0.0265,$$

Now based on equation (4-3),

$$e^+ = 233.32,$$

Now G can be evaluated from figure 4.17 (b) but to be more accurate an alternative relation presented by Han et al (1989) for $Pr = 0.7$ can be used as follow:

$$G = C(e^+)^n \quad (4-7)$$

For our case $n = 0.35, C = 2.24$ so

$$G = 15.10,$$

Now based on equation (4-2),

$$St_r = 0.00612,$$

St is related to Nu and h as following:

$$St = \frac{Nu}{Re Pr} = \frac{h}{\rho V C_p} \quad (4-8)$$

Based on the above equation (4-8):

$$h = 388.53 \text{ W/m}^2 \cdot \text{k}$$

Taking $f_s = 0.011$ then according to equation (4-4):

$$\bar{f} = 0.0162$$

Therefore friction factor for the two-sided orthogonal ribbed channel is 0.0162.

Table 4.2 shows h value for other e/D_h ratios.

Table 4-2: Friction factor, Nu number and h value for different rib blockage ratios, e/D_h when $\alpha=90^\circ$.

R(e+)	e/D	Re	\bar{f}	e+	G(e+,Pr)	Str	Nu_{ribbed}	$h_{ribbed} (W / m^2 .K)$
5	0.042	32192.12	0.0144	139.30	12.61	0.00595	134.10	377.71
5	0.047	32192.12	0.0148	160.54	13.25	0.00600	135.28	381.04
5	0.063	32192.12	0.0162	233.32	15.10	0.00612	137.94	388.53
5	0.078	32192.12	0.0173	307.78	16.64	0.00619	139.52	392.98

Note that for a smooth channel as calculated before, $h_{smooth} = 224.22(W / m^2 .K)$ and $Nu_{smooth} = 79.60$. Figure 4.18, shows temperature distribution in this case.

T1	T2	T3	T4	T5	T6						
1398.24	1395.92	1390.24	1386.71	1402.10	1428.60						
T7	T8	T9	T10	T11	T12	T13	T14	T15			
1364.36	1361.10	1352.00	1339.65	1360.80	1389.96	1447.99	1489.21	1519.07			
T16	T17	T18	T19	90 Ribbed	T20	T21	T22	T23			
1336.97	1332.14	1317.00	1288.32		1425.96	1469.60	1505.49	1536.69			
T24	T25	T26	T27		T28	T29	T30	T31	T32		
1319.25	1313.49	1295.56	1263.40		1413.40	1457.73	1495.67	1528.69	1556.09		
T33	T34	T35	T36		T37	T38	T39	T40	T41		
1313.05	1307.01	1288.33	1255.59		1407.76	1452.26	1490.75	1523.47	1548.95		
T42	T43	T44	T45		T46	T47	T48	T49	T50	T51	
1318.94	1313.16	1295.18	1262.99		1408.16	1452.80	1491.61	1525.48	1556.51	1585.10	
T52	T53	T54	T55		T56	T57	T58	T59	T60	T61	
1336.38	1331.50	1316.23	1287.41		1414.37	1459.17	1497.40	1530.33	1559.81	1586.12	
T62	T63	T64	T65	T66	T67	T68	T69	T70	T71	T72	
1363.58	1360.24	1350.84	1337.87	1357.14	1384.02	1426.65	1472.10	1508.48	1538.65	1565.38	
T73	T74	T75	T76	T77	T78	T79	T80	T81	T82		
1397.46	1395.04	1389.02	1384.73	1398.48	1422.54	1457.06	1494.11	1525.77	1550.19		

Figure 4.18: Temperature (K) distribution in the cross section of GT blade surrounding the 90° ribbed cooling channel at root of the blade.

4.3.2 Introducing 60° Ribs

According to figure 4.17 (a) for $\alpha = 60^\circ$, R can be estimated as 3.25. Using this value in equation (4-1) and substituting other values ($Re=32192.12$, $W = 9mm$, $H = 18mm$) and assuming rib blockage ratios, $e/D_h=0.042$, friction factor for four-sided ribbed channel is calculated as:

$$f = 0.0316,$$

Now based on equation (4-3),

$$e^+ = 169.94,$$

Now G can be evaluated from figure 4.17 (b) but to be more accurate an alternative relation presented by Han et al (1989) for $Pr = 0.7$ can be used as follow:

$$G = C(e^+)^n, \quad n = 0.35 \text{ and } C = 1.80 \text{ if } 30^\circ < \alpha < 90^\circ \quad (4-9)$$

For our case $\alpha = 60^\circ$, calculating G base on equation (4-9),

$$G = 10.86,$$

Now based on equation (4-2),

$$St_r = 0.00807,$$

Based on the equation (4-8):

$$h = 512.48 \text{ W/m}^2.\text{k}$$

Taking $f_s = 0.011$ then according to equation (4-4):

$$\bar{f} = 0.0179$$

Therefore friction factor for the two-sided 60° ribbed channel is 0.0179.

Table 4.3 shows h value for other e/D_h ratios.

Table 4-3: Friction factor, Nu number and h value for different rib blockage ratios, e/D_h when $\alpha=60^\circ$.

R(e+)	e/D	Re	\bar{f}	e+	G(e+,Pr)	Str	Nu_{ribbed}	$h_{ribbed} (W / m^2 .K)$
3.25	0.042	32192.12	0.0179	169.94	10.86	0.00807	181.95	512.48
3.25	0.047	32192.12	0.0187	197.14	11.44	0.00821	185.07	521.27
3.25	0.063	32192.12	0.0212	292.14	13.13	0.00856	192.97	543.53
3.25	0.078	32192.12	0.0236	391.83	14.55	0.00881	198.57	559.32

Now G can be evaluated from figure 4.17 (b), but to be more accurate we refer to equation (4-9),

$$G = 10.57,$$

Now based on equation (4-2),

$$St_r = 0.00761,$$

Based on the equation (4-8):

$$h = 482.91 \text{ W/m}^2.\text{k}$$

Taking $f_s = 0.011$ then according to equation (4-4):

$$\bar{f} = 0.0163$$

Therefore friction factor for the two-sided 45° ribbed channel is 0.0163.

Table 4.4 shows h value for other e/D_h ratios.

Table 4-4: Friction factor, Nu number and h value for different rib blockage ratios, e/D_h when $\alpha=45^\circ$.

$R(e+)$	e/D	Re	\bar{f}	$e+$	$G(e+,Pr)$	Str	Nu_{ribbed}	$h_{ribbed} (W / m^2 .K)$
3.9	0.042	32192.12	0.0163	157.11	10.57	0.00761	171.45	482.91
3.9	0.047	32192.12	0.0170	181.75	11.12	0.00773	174.14	490.50
3.9	0.063	32192.12	0.0189	267.12	12.72	0.00802	180.80	509.25
3.9	0.078	32192.12	0.0207	355.74	14.07	0.00823	185.35	522.07

Note that for a smooth channel as stated before, $h_{smooth} = 224.22(W / m^2 .K)$ and $Nu_{smooth} = 79.60$. Figure 4.20, shows temperature distribution in this case.

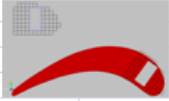
T1	T2	T3	T4	T5	T6																	
1335.18	1332.31	1325.21	1320.44	1338.30	1370.11																	
T7	T8	T9	T10	T11	T12	T13	T14	T15														
1294.27	1290.29	1279.08	1263.58	1287.91	1322.74	1387.46	1438.85	1475.93														
T16	T17	T18	T19	45 Ribbed				T20	T21	T22	T23											
1261.33	1255.51	1237.25	1202.70					1360.42	1414.67	1459.23	1497.92											
T24	T25	T26	T27					T28	T29	T30	T31	T32										
1240.05	1233.15	1211.69	1173.32					1345.22	1400.18	1447.20	1488.12	1522.05										
T33	T34	T35	T36					T37	T38	T39	T40	T41										
1232.57	1225.35	1203.06	1164.09					1338.54	1393.63	1441.27	1481.75	1513.27										
T42	T43	T44	T45					T46	T47	T48	T49	T50	T51									
1239.55	1232.61	1211.09	1172.68					1339.30	1394.52	1442.49	1484.35	1522.71	1558.05									
T52	T53	T54	T55					T56	T57	T58	T59	T60	T61									
1260.38	1254.47	1236.01	1201.25					1347.30	1402.65	1449.82	1490.46	1526.83	1559.32									
T62	T63	T64	T65	T66	T67	T68	T69	T70	T71	T72												
1293.02	1288.90	1277.21	1260.70	1281.94	1312.81	1363.29	1418.98	1463.68	1500.83	1533.78												
T73	T74	T75	T76	T77	T78	T79	T80	T81	T82													
1333.92	1330.89	1323.24	1317.22	1332.38	1360.19	1401.19	1446.28	1485.09	1515.15													

Figure 4.20: Temperature (K) distribution in the cross section of GT blade surrounding the 45° ribbed cooling channel at root of the blade.

4.3.4 Introducing 30° Ribs

According to figure 4.17 (a) for $\alpha = 30^\circ$, R can be estimated as 5.2. Using this value in equation (4-1) and substituting other values ($Re=32192.12$, $W = 9mm$, $H = 18mm$) and assuming rib blockage ratios, $e/D_h=0.042$, friction factor for four-sided ribbed channel is calculated as:

$$f = 0.0204,$$

Now based on equation (4-3),

$$e^+ = 136.49,$$

Now G can be evaluated from figure 4.17 (b) but to be more accurate we refer to equation (4-9),

$$G = 10.06,$$

Now based on equation (4-2),

$$St_r = 0.00684 ,$$

Based on the equation (4-8):

$$h = 433.96 \text{ W/m}^2.\text{k}$$

Taking $f_s = 0.011$ then according to equation (4-4):

$$\bar{f} = 0.0144$$

Therefore friction factor for the two-sided 30° ribbed channel is 0.0144.

Table 4.5 shows h value for other e/D_h ratios.

Table 4-5: Friction factor, Nu number and h value for different rib blockage ratios, e/D_h when $\alpha=30^\circ$.

R(e+)	e/D	Re	\bar{f}	e+	G(e+,Pr)	Str	Nu_{ribbed}	$h_{ribbed} (W / m^2 .K)$
5.2	0.042	32192.12	0.0141	136.49	10.06	0.00684	154.07	433.96
5.2	0.047	32192.12	0.0145	157.20	10.57	0.00693	156.15	439.83
5.2	0.063	32192.12	0.0158	228.07	12.04	0.00715	161.09	453.73
5.2	0.078	32192.12	0.0169	300.41	13.26	0.00729	164.23	462.58

Figure 4.21, shows temperature distribution in this case:

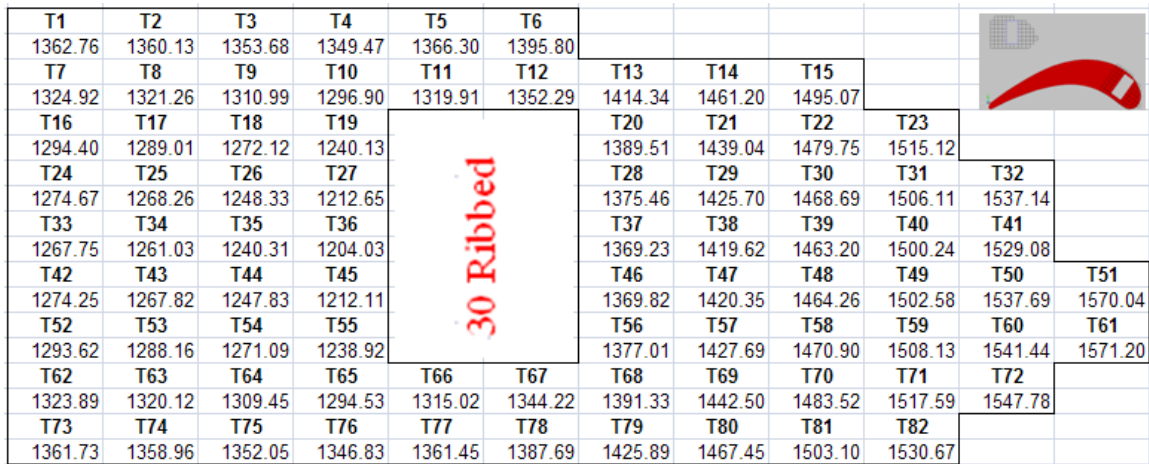


Figure 4.21: Temperature (K) distribution in the cross section of GT blade surrounding the 30° ribbed cooling channel at root of the blade.

4.3.4 Comparison between Different Rib Angles

As it was shown in the pervious section maximum convection heat transfer coefficient h and Nu occur when e/D_h is maximum (look at the tables 4-2 to 4-5). It should be noted that when rib blockage ratio (e/D_h) increases friction factor also rises, therefore an enhancement of heat transfer is achieved with penalty of increase in the friction factor.

Comparing different rib angles, by looking at the tables 4-2 to 4-5, it is obvious that maximum Nu value and h is achieved when 60° ribs are used in the channel with a rib blockage ratio of 0.078. Comparing with smooth channel an enhancement of 149.45% is achieved with penalty of increase in the friction factor by 114.5%.

Table 4-6, compares maximum and minimum temperature, heat transfer per length as well as increment in air temperature when leaving the channel.

Table 4-6: Comparison between different rib angles for maximum and minimum temperature, heat transfer per length and increment in air temperature when leaving the channel.

Rib Angle	Max Temp. (K)	Min Temp. (K)	q (W/m)	ΔT air (K) across channel
90	1586.12	1255.59	20693.28	428.56
60	1552.26	1140.81	26743.46	553.86
45	1559.32	1164.09	25482.49	527.74
30	1571.20	1204.03	23361.36	483.82
Smooth	1627.85	1407.91	13196.91	259.00

For further discussion please refer to section 4.4, discussion on the results.

4.4 DISCUSSION ON THE RESULTS

1. Accuracy of the finite difference solution may be improved by refining the grid. For example if we halve the grid spacing ($\Delta x=1.5\text{mm}$).
2. In the gas turbine industry there is great interest in adopting measures that reduce blade temperatures. Such measures could include use of a different alloy o larger thermal conductivity and/or increasing coolant flow through the channel, thereby increasing h_i . Using the finite-difference solution, the following results are obtained for parametric variations of k and h_i .

Table 4-7: Comparison between effect of *thermal conductivity* and *conduction coefficient* on the blade cooling in smooth channel.

k(W/m.K)	h_i(W/m².K)	T_{max} (K)	q (W/m)
25	200	1634.6	11976.86
50	200	1615.68	12243.68
25	400	1584.56	20972.26
50	400	1549.31	21775.01

According to the table 4.7 it is obvious that increasing the k and h_i reduce temperature in blade but effect of change in h_i is far more significant than that of k .

3. Temperature of compressed air entering the bottom of the channel will increase because q is transferred to the air passing in the channel. This change in temperature depends on air mass flow rate that also changes the h_i value. For our case, considering the air mass flow rate in a smooth channel as 0.01 kg/s the temperature difference between air entering and leaving the channel at the tip of blade will be 259 K. According to Fig 4.10 by increasing air mass flow rate the out let temperature will decrease and tends to approach air inlet temperature (400 K).
4. According to Fig 4.6, as expected the maximum temperature exists at the location furthest removed from the coolant means the leading edge (node 61), that is why this part of the blade is the most critical and other cooling techniques are also used

to cool the leading edge even further (impingement cooling). Minimum temperature is 1433.68 K and exists at node 36 in contact with the left side of the air channel and far from leading edge comparing this value with hot gas temperature a difference of 270 K is obtained.

5. Table below shows maximum temperature in each segment of the blade with smooth channel, according to this table temperature difference is not more than 6 K along the blade tip and can be neglected. Changes of minimum temperature is around 20 K along the blade:

Table 4-8: Variations of max & min temperature along the height of the blade.

Segment	Max Temp (K).	Min Temp (K).
1	1627.85	1413.05
2	1629.24	1414.19
3	1631.13	1422.34
4	1633.49	1432.24

6. According to Fig 4.11, there is an almost linear correlation between air mass flow rate and convection coefficient. Properties of air can be considered on changed because the error is only 2.12%.
7. According to Fig 4.12, local convection heat transfer increases through the channel.
8. According to Fig 4.13 the temperature on the top blade surface continuously decreases and reaches its minimum value at $x=24\text{mm}$ (node 4) and after passing the air channel again increases (same explanation applies for Fig 4.14) this shows the significance of use of internal cooling.
9. If we draw a line that divides the cross section into two equal parts (chamber line) and move along it the temperature continuously decreases and there will be a sharp decrease after passing the channel (between $x=51$ to $x=24$, about 100K), temperature of whole nodes after channel are less than nodes before that. (Fig 4.16)

Discussion on results for ribbed channel.

10. Referring to tables 4-2 to 4-5, conclusion is that, increasing rib blockage ratio for each rib angle rises both Nu value (therefore h) and friction factor, \bar{f} .
11. Knowing that $Nu_{smooth} = 79.60$ and $h_{smooth} = 224.22$ (W/m².K) and comparing these values with tables 4-2 to 4-5, it is found that introducing the ribs in the channel regardless of the angle will increase heat transferred to the air, friction factor will always increase as well. Ribs mostly disturb only the near wall flow, and consequently the pressure drop penalty by ribs is acceptable for blade cooling design, so introducing the ribs in the channel is always recommended. (Similar conclusion can be obtained by referring to table 4-6 and figures 4.18 to 4.21).
12. Last row of tables 4-2 to 4-5, shows the maximum h value for each rib angle, comparing this values, 60° ribbed channel will result in the maximum heat transfer enhancement comparing this value with smooth channel h value is increased by 149.45%. Comparing friction factor in this case and smooth channel it is found that introducing 60° ribs will have a penalty of increase in the friction factor by 114.5%.
13. By looking at the tables 4-3 and 4-4 and comparing h values, using a 45° ribbed channel with rib blockage ratio of 0.078 instead of 60° ribbed channel with rib blockage ratio of 0.042 or 0.047 is justified in term of heat transfer enhancement.
14. Comparing tables 4-2 and 4-5, we will notice that h value for 30° ribbed channel regardless of rib blockage ratio is always greater than that of 90° ribbed channel and at the same time 30° ribbed channel generates smaller friction factors, so there is no point of using 90° ribs and it is not recommended at all when other angles are available.

15. According to discussed matters in 12, 13 and 14 the priority of using the ribs in terms of heat transfer enhancement is given here. Note that the second number is rib blockage ratio.

- a) 60° , 0.078
- b) 60° , 0.063
- c) 45° , 0.078
- d) 60° , 0.047
- e) 60° , 0.042
- f) 45° , 0.063
- g) 45° , 0.047
- h) 45° , 0.042
- i) 30° , 0.078
- j) 30° , 0.063
- k) 30° , 0.047
- l) 30° , 0.042
- m) 90° , 0.078
- n) 90° , 0.063
- o) 90° , 0.047
- p) 90° , 0.042

CHAPTER 5

CONCLUSION AND RECOMMENDATION

As a conclusion, cooling system is very essential for Gas Turbines and has a direct effect on Gas Turbine efficiency. There are different cooling techniques (internal and external) available. Internal cooling is achieved by passing the compressed air through the internal channel provided in the blade and is enhanced by manufacturing the ribs inside the air passage. Internal cooling for the leading edge of the blade is analyzed in the present work with help of finite difference method.

According to the obtained results leading edge is the most critical part of the blade. The effect of increasing heat transfer convection coefficient h in the air channel on cooling is found to be far more effective than increasing thermal conductivity of the blade. (i.e. the material).

By increasing the mass flow rate of air in the channel heat transfer convection coefficient will increase also at the same time air outlet temperature will decrease and approaches to air inlet temperature. In low mass flow rates the change in air properties in the channel can be neglected with good approximation.

Introducing ribs in the channel will result in heat transfer enhancement and pressure drop inside the passage. Ribs mostly disturb only the near wall flow, and consequently the pressure drop penalty by ribs is acceptable for blade cooling design, so introducing the ribs in the channel is always recommended. Among the rib angles, α of 90° , 60° , 45° and 30° and ribs blockage ratios, e/D_h ranging from 0.042 to 0.078 studied in this work, 60° ribbed channel with rib blockage ratio of 0.078 is recommended to be used for the gas turbine blade. An enhancement of 149.45% is achieved with penalty of increase in the friction factor by 114.5%. Channels with 30° ribs are recommended to be used when pressure drop in the channel is important. Channels with 90° ribs do not have any advantages in terms of heat transfer enhancement or pressure drop reduction comparing

with other ribs so using 90° ribs is not recommended at all when other ribs are available.
Best ribs for heat transfer enhancement are 60°, 0.078; 60°, 0.063; 45°, 0.078.

REFERENCES

1. Al-Hadhrami, L., and Han, J. C. 2002. Effect of rotation in two-pass square channels with parallel and crossed 45 angled rib turbulators. *Proceeding of 9th International Symposium on Transport Phenomena and Dynamics of Rotating Machinery*, ISROMAC-9, HT-ABS-031; *International Journal of Heat and Mass Transfer*, February 2003, 46:653–669.
2. Aminossadati S.M. and Mee D.J. (1995) “Simulation of aerodynamic loss for trailing-edge coolant ejection in gas turbine blades”; Presented at the Twelfth Australasian Fluid Mechanics Conference; The University of Sydney; Australia.
3. Ammari, H.D., Hay, N., Lampard, D., 1990, “The Effect of Density Ratio on the Heat Transfer Coefficient from a Film Cooled Flat Plate”, *ASME Journal of Turbomachinery*, vol. 112, pp. 444-450.
4. Ammari, H.D., Hay, N., Lampard, D., 1991, “Effect of Acceleration on the Heat Transfer Coefficient on a Film Cooled Surface”, *ASME Journal of Turbomachinery*, vol. 113, pp. 464-470.
5. Andreopoulos, J., Rodi, W., 1983, “Experimental investigation of jets in a crossflow”, *J. Fluid Mech.*, vol. 138, pp. 93-127.
6. Azad, G. S., Uddin, J. M., Han, J. C., Moon, H. K., and Glezer, B. 2001. “Heat transfer in a two-pass rectangular rotating channel with 45-degree angled rib turbulators”. *ASME Paper No. 2001-GT-186*; *ASME Journal of Turbomachinery*, April 2002, 124:251–259.
7. Bathie W.W. (1995) “Fundamentals of gas turbines”; Second Edition; Iowa State University of Science and Technology”; USA
8. Bogard, D.G., Schmidt, D.L., Tabbita, M., 1998, “Characterization and Laboratory Simulation of Turbine Airfoil Surface Roughness and Associated Heat Transfer”, *ASME Journal of Turbomachinery*, vol. 120, pp. 337-342.
9. Bons, J.P., MacArthur, C.D., Rivir, R.B., 1996, “The Effect of High Free-Stream Turbulence on Film Cooling Effectiveness”, *ASME Journal of Turbomachinery*, vol. 118, pp. 814-825
10. Bunker, R.S., 2000, “Effect of Partial Coating Blockage on film cooling effectiveness”, *ASME Turbo Expo 2000*, 2000-GT-0244.
11. Cohen H., Rogers G.F.C., Saravanamuttoo H.I.H. (1996). “Gas turbine theory”; 4th Edition, Longman Group Limited; England.

12. Crabb, D., Durao, D.F.G., Whitelaw, J.H., 1981, "A round jet normal to a cross flow", *J. Fluids Engng*, vol. 103, pp. 142-152.
13. Dewill, Bergman, Lavine, 2007, "Introduction to heat transfer", 5th edition
14. Eriksen, V.L., Goldstein R.J., 1974, "Heat transfer and Film Cooling Following Injection Through Inclined Circular Holes" *ASME Journal of Heat transfer*, vol. 96, pp. 239-245.
15. Goldstein, R.J., 1971, "Film Cooling", *Advances in Heat Transfer*, vol. 7, pp. 321-379.
16. Goldstein, R.J., Eckert, E.R.G., Burgraff, F., 1974, "Effects of Hole Geometry and Density of Three-Dimensional Film Cooling Performance", *International Journal of Heat and Mass transfer*, vol. 17, pp. 595-605.
17. Griffith, T. S., Al-Hadhrami, L., and Han, J. C. 2001." Heat transfer in rotating rectangular cooling channels (AR=4) with angled ribs". *AIAA Paper No. 2001-2820*; *ASME Journal of Heat Transfer*, August 2002, 124(4):617–625.
18. Han, J.C 1988. "Heat Transfer and Friction Characteristics in Rectangular Channels with Rib Turbulators." *ASME Journal of Heat and Mass Transfer*, vol. 110, May, pp. 321-328.
19. Han, J.C., Park, J.S and Lei, C.K., 1989. "Augment Heat Transfer in Rectangular Channels of Narrow Aspect Ratios with Rib Turbulators." *International Journal of Heat and Mass Transfer*, vol. 110, May, pp.321-328.
20. Han, J. C., Zhang, Y. M., and Kalkuehler, K., 1993. "Uneven wall temperature effect on local heat transfer in a rotating two-pass square channel with smooth walls". *ASME Journal of Heat Transfer* 114(4):850–858.
21. Han, J.C, Sandip Dutta and Srinath V.Ekkad, 2000, "Gas turbine heat transfer and cooling technology".
22. Han, J.C., 2002. "Recent studies in Turbine Blade Cooling", 9th International Symposium on Rotating Machinery.
23. Hay et al., 1985. N. Hay, D. Lampard and C.L. Saluja, Effect of cooling films on the heat transfer coefficient on a flat plate with zero mainstream pressure gradient. *ASME J. Eng. Gas Turbines Power* 107 (1985), pp. 105–110

24. Johnathan Green, 2007, "Micro-Scale Film Cooling For Gas Turbine Applications", MSc Thesis, Cranfield University
25. Johnson, B. V., Wagner, J. H., Steuber, G. D., and Yeh, F. C. 1994 "Heat transfer in rotating serpentine passages with trips skewed to the flow". *ASME Journal of Turbomachinery* 116(1):113–123.
26. Ligrani, P.M., Wigle, J.M., Ciriello, S., Jackson, S.W., 1994a, "Film-Cooling from Holes with Compound Angle orientations. Part 1: Results Downstream of Two Staggered Rows of Holes with 3D Spanwise Spacing", *ASME Journal of Heat Transfer*, vol. 116, pp. 341-352.
27. Ligrani, P.M., Wigle, S., Jackson, S.W., 1994b, "Film-Cooling from Holes with Compound Angle orientations. Part 2: Results Downstream of a Single Row of Holes with 6D Spanwise Spacing", *ASME Journal of Heat Transfer*, vol. 116, pp. 353-362.
28. Liou, T.-M., and Hwang, J.-J., 1992. "Turbulent heat transfer augmentation and friction in periodic fully developed channel flows". *J.Heat Transfer*, 114:56.64.
29. Leylek, J.H., Zerkle, R.D., 1994, "Discrete-jet Film Cooling: A Comparison of Computational Results with Experiments", *ASME Journal of Turbomachinery*, vol. 116, pp. 358-368.
30. Metherwan P. Boyce, 2002, "Gas Turbine engineering hand book 2nd Edition", Gulf Professional publishing
31. Moussa, Z.M., Trischka, J.W., Eskinazi, S., 1977, "The near field in the mixing of a round jet with a cross stream", *J. Fluid Mech.*, vol. 80, pp. 49-80.
32. Mohamed Fathelrahman, 2009. "Ribbed double pipe heat exchanger, analytical analysis." FYP report, Universiti Teknologi PETRONAS
33. Mohammed S.Altorairi, 2003, "Film cooling from cylindrical holes in transverse slots", King Fahad University
34. Parsons, J. A., Han, J. C., and Zhang, Y. M. 1994. "Wall heating effect on local heat transfer in a rotating two-pass square channel with 90-degree rib turbulators". *International Journal of Heat and Mass Transfer* 37(9):1411–1420.
35. Pedersen, D.R., Eckert, E.R.G., Goldstein, R.J., 1977, "Film-Cooling with Large Density Differences Between the Mainstream and Secondary Fluid Measured by

- the Heat-Mass Transfer Analogy”, ASME Journal of Heat Transfer, vol. 99, pp. 620-627.
36. Rolls Royce (1973). “The jet engine”; Rolls Royce Limited; 3rd Edition with Revision, Publication Reference T.S.D. 1302.
 37. Sen, B., Schmidt, D.L. Bogard, D.G., 1996, “Film Cooling with Compound Angle Holes: Heat Transfer” ASME Journal of Turbomachinery, vol. 118, pp. 800-806.
 38. Seo, H.J., Lee, J.S., Ligrani, P.M., 1998, “The Effect of Injection hole length on film cooling with bulk flow pulsations”, International Journal of Heat and Mass Transfer, vol. 41, pp. 3515-3528.
 39. Wagner, J. H., Johnson, B. V., and Kopper, F. C. 1991. “Heat transfer in rotating serpentine passages with smooth walls”. *ASME Journal of Turbomachinery* 113:321–330.
 40. Webb, R.L., Eckert, E.R.G., and Goldstein, J., 1971, “Heat transfer and friction in tubes with roughness”. *Int. J. Heat and Mass Transfer*, 14:601.617.
 41. Willett, F. T., and Bergles, A. E. 2000.” Heat transfer in rotating narrow rectangular ducts with heated sides oriented at 60-degree to the R-Z plane”. *ASME Paper No. 2000-GT-224*.